JOURNAL OF PETROLOGY | VOLUME 44 | NUMBER 3 | PAGES 457–489 | 2003

Trace Element and Sr, Nd, Pb and O Isotope Variations in Medium-K and High-K Volcanic Rocks from Merapi Volcano, Central Java, Indonesia: Evidence for the Involvement of Subducted Sediments in Sunda Arc Magma Genesis

R. GERTISSER* AND J. KELLER

INSTITUT FÜR MINERALOGIE, PETROLOGIE UND GEOCHEMIE, UNIVERSITÄT FREIBURG, ALBERTSTRASSE 23B, D-79104 FREIBURG, GERMANY

RECEIVED FEBRUARY 1, 2002; ACCEPTED SEPTEMBER 9, 2002

Merapi volcano (Central Java), located within the Quaternary volcanic front of the Sunda arc, is one of the most active volcanoes of the Indonesian archipelago. During the Holocene, Merapi erupted basalts and basaltic andesites of medium-K affinity during its earlier stages of activity and high-K compositions over the past ~1900 years. Merapi lavas and pyroclastic rocks are characterized by enrichment in large ion lithophile elements (LILE) and light rare earth elements (LREE) relative to high field strength elements (HFSE) and higher $^{87}Sr/^{86}Sr$, $^{206}Pb/^{204}Pb$, $^{207}Pb/^{204}Pb$ and $^{208}Pb/^{204}Pb$ ratios and lower $^{143}Nd/^{144}Nd$ ratios compared with Indian Ocean mid-ocean ridge basalt (MORB). Merapi high-K series rocks are enriched in LILE and LREE and slightly depleted in heavy REE (HREE) and HFSE compared with rocks from the medium-K series. The increase in K_2O is accompanied by a marked increase in $^{87}Sr/^{86}Sr$ and a general decrease in $^{143}Nd/^{144}Nd$, but not by systematic variations in $\delta^{18}O$ values. The low $\delta^{18}O$ nature of the Merapi magmas, and the lack of any major shift in isotopic compositions along the evolutionary trend of the two individual series, precludes extensive crustal assimilation during magma ascent and differentiation, emphasizing the importance of subducted continental material in the genesis of Merapi magmas. The compositional contrast between medium-K and high-K series volcanics largely reflects variable contributions from subducted sediment to the mantle wedge, which was similar to a MORB-source mantle before any subduction-related modification. The temporal change in the K_2O content of the magmas reflects compositional variation in the mantle wedge rather than intracrustal processes occurring within the shallow volcanic system.

KEY WORDS: *arc magma series; geochemistry; Merapi; sediment subduction; Sunda arc*

INTRODUCTION

Understanding the origin of magmatic rocks associated with island arcs and active continental margins is of prime interest in igneous petrology. The suites of rocks formed above Benioff zones commonly belong to distinct magmatic series that may cover most of the compositional range between basalt and rhyolite but differ often in their potassium content. In general, volcanic rocks with intermediate K_2O contents of the calc-alkaline series dominate volcanic zones associated with convergent plate boundaries involving continental crust. However, subduction-related rocks with lower and higher K_2O contents also occur, giving rise to

*Corresponding author. Present address: Department of Earth Sciences, The Open University, Walton Hall, Milton Keynes MK7 6AA, UK. Telephone: +44 (0)1908 653012. Fax: +44 (0)1908 655151. E-mail: r.gertisser@open.ac.uk

characteristic magma series in arc settings that range from tholeiitic to calc-alkaline, high-K calc-alkaline, shoshonitic and in some cases K-rich alkaline or leucititic series (Wilson, 1989).

It is generally accepted that multiple source components are required to explain the range of geochemical and isotopic characteristics of subduction-related volcanic rocks (Arculus & Powell, 1986; Ellam & Hawkesworth, 1988; Stolz *et al*., 1990; Hawkesworth *et al*., 1993). One of these components is the mantle wedge above the subducted lithospheric slab, which is usually inferred to have the geochemical and isotopic characteristics of mid-ocean ridge basalt (MORB) source (Perfit *et al*., 1980) or even depleted MORB-source mantle (McCulloch & Gamble, 1991; Woodhead *et al*., 1993; Elliott *et al*., 1997) before any modification by components derived from the subducted slab. However, in some cases, the trace element and isotopic characteristics of arc magmas resemble those of ocean island basalts (OIB) rather than MORB, implying the existence of more enriched mantle source components in arc magma genesis (Morris & Hart, 1983; Stolz *et al*., 1990; Edwards *et al*., 1994). Although the mantle wedge is considered to be volumetrically the most significant source of the majority of basaltic arc magmas (Arculus & Powell, 1986), satisfactory interpretation of the trace element and isotopic characteristics of island arc volcanic rocks requires the involvement of additional components from the subducted basaltic oceanic crust and associated sediments (Kay, 1980; Whitford & Jezek, 1982; Tera *et al*., 1986; White & Dupré, 1986; Ellam & Hawkesworth, 1988; McDermott *et al*., 1993; Vroon *et al*., 1993, 2001; Gamble *et al*., 1996, 1997; Price *et al*., 1999; Turner & Foden, 2001). Varying contributions of these subduction-related components to the source region of arc magmas, the transfer mechanisms of specific trace elements from the slab to the sub-arc mantle (Ellam & Hawkesworth, 1988; Elliott *et al*., 1997; Hoogewerff *et al*., 1997), and the composition and amount of subducted sediments involved in the genesis of arc magmas (Plank & Langmuir, 1998) are the most important parameters that determine the compositional diversity of primary arc magmas. Further complexities may arise from the modification of mantle-derived magmas by assimilation of crustal material during ascent or storage in a crustal magma reservoir (Davidson, 1987; Hildreth & Moorbath, 1988; Davidson & Harmon, 1989; Davidson *et al*., 1990; Ellam & Harmon, 1990; Thirlwall *et al*., 1996).

The large number of factors affecting magma compositions in volcanic arc settings precludes a universally valid model for the petrogenesis of arc magmas. Therefore, detailed stratigraphic, geochemical and isotopic studies of individual volcanic centres are required to assess the relative importance and contributions of the various potential source components and processes involved in magma genesis and evolution. Lessons learnt from investigations of individual volcanoes may be used to evaluate the processes of magma generation on a regional scale within a particular arc setting.

In this paper we present new major element, trace element, and radiogenic (Sr, Nd, Pb) and stable (O) isotope data for a stratigraphically well-characterized suite of lavas and pyroclastic rocks from Merapi volcano, in the central part of the Sunda arc. This arc provides a classic example of subduction-related volcanism, because the K_2O content of the volcanic rocks having the same degree of differentiation increases regularly with depth to the underlying Benioff zone (Whitford & Nicholls, 1976; Whitford *et al*., 1979; Nicholls *et al*., 1980; Hutchison, 1982; Wheller *et al*., 1987; Stolz *et al*., 1990; Edwards *et al*., 1993). Merapi, currently one of the most active volcanoes in Indonesia, is situated within the active volcanic front of the Sunda arc and ~190 km above the subducting slab (Whitford & Nicholls, 1976). During the Holocene, Merapi erupted basalts and basaltic andesites of medium-K and high-K affinity (Andreastuti, 1999; Gertisser, 2001; Gertisser & Keller, 2003) that are typical of the volcanic associations of most island arcs and active continental margins. Similar volcanic products account for >90% of the eruptive rocks of the Sunda arc (Whitford *et al*., 1979). The eruption of medium-K and high-K lavas and pyroclastic rocks over a very short time from the same volcanic complex clearly restricts the role that changes in crustal thickness or composition or depth to the Benioff zone may have had on the compositional variations observed in subduction-zone volcanoes. Moreover, it provides an excellent opportunity to evaluate the genetic relationship between geochemically distinct arc volcanic suites and the possible roles of subvolcanic (intracrustal) vs mantle wedge processes involved in generating the geochemical variations observed in different arc series.

TECTONIC AND GEOLOGICAL SETTING

The active volcanoes of the Indonesian archipelago are related to several distinct subduction-zone systems, namely the Sunda, Banda, Sangihe and Halmahera arc systems (Fig. 1). Merapi volcano, located 25 km north of the city of Yogyakarta in Central Java, belongs to the Sunda volcanic arc, which forms a continuous geological structure from the northern tip of Sumatra in the west to the island of Flores in the east. The Quaternary volcanism of the Sunda arc is related

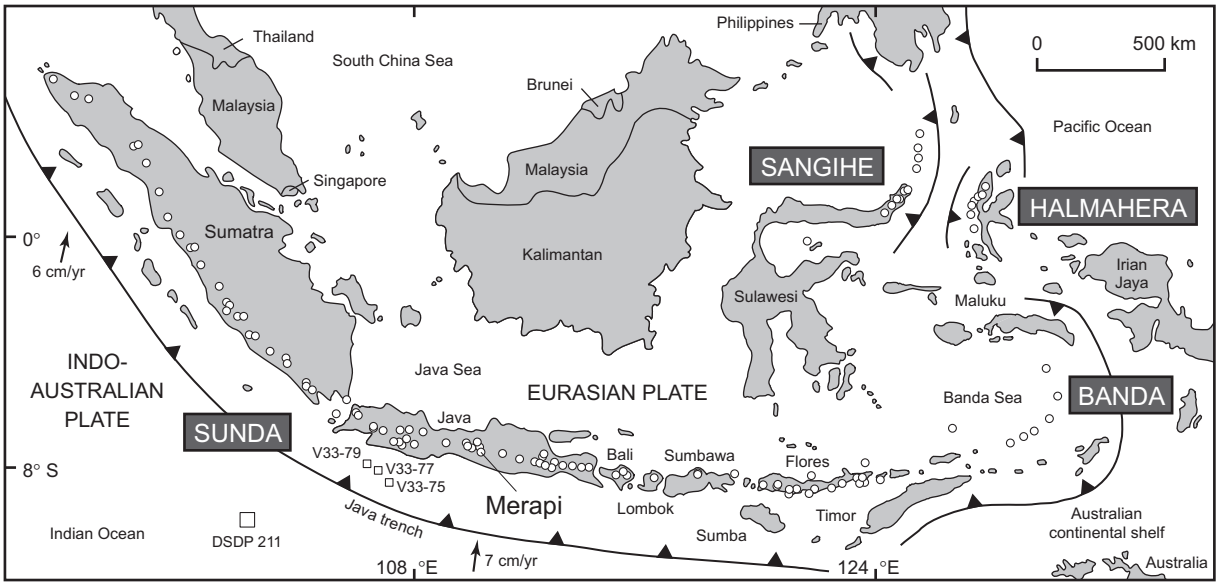

Fig. 1. Map of the Indonesian subduction-zone system showing the general tectonic setting (after Hamilton, 1979) and distribution of active volcanoes (◯) (after Simkin & Siebert, 1994). Arrows indicate the direction of the Indo-Australian plate motion relative to the Eurasian plate. Along the Sunda arc, oceanic lithosphere is subducting beneath the Eurasian plate, whereas east of Flores, the Banda arc is colliding with the northward-migrating passive continental lithosphere of Australia. The convergence rates of the Indo-Australian and Eurasian plates are from Widiyantoro & Van der Hilst (1997). The locations of Indian Ocean sediment samples [Deep Sea Drilling Project (DSDP) Site 211; R.V. *Vema* core and dredge sites near Java], used to assess subducted sediment compositions, are also shown.

to the northward subduction of the Indo-Australian plate beneath the Eurasian plate at a rate of 6 cm/yr near Sumatra and 7 cm/yr near Java (Hamilton, 1979; Jarrard, 1986; Widiyantoro & Van der Hilst, 1996, 1997). Along the Sunda arc, both the age of the subducting lithosphere and the composition and thickness of the overriding plate change significantly; the latter reflecting the progressive eastward migration of a series of subduction zones in the evolution of the Indonesian archipelago since the late Palaeozoic (Katili, 1975). In Sumatra, oceanic lithosphere younger than 100 Ma is subducting obliquely beneath a 25 km thick, mature continental crust consisting of late Palaeozoic, Mesozoic and Tertiary rocks (Van Bemmelen, 1949; Katili, 1975), whereas in Java and the eastern Sunda arc, older oceanic lithosphere is subducting almost perpendicular to the arc front (Hamilton, 1979; Puspito & Shimazaki, 1995; Widiyantoro & Van der Hilst, 1996, 1997). The 20 km thick, quasi-continental crust beneath Java has a seismic velocity structure intermediate between typical continental and oceanic crust (Curray *et al*., 1977; Jarrard, 1986) and consists of Cretaceous and Tertiary rocks (Van Bemmelen, 1949). East of Java in the eastern Sunda arc, the arc crust is oceanic in character (Hamilton, 1979; Edwards *et al*., 1993). Seismic data indicate a crustal thickness of 5–10 km beneath the island of Flores at the eastern end of the Sunda arc (Curray *et al*., 1977; Stolz *et al*., 1990).

Compared with most volcanic arcs the Java–Bali sector of the Sunda arc is characterized by a relatively simple plate tectonic setting. Earthquake foci define a north-dipping Benioff zone that can be traced from the 6–7 km deep Java trench south of the arc to a depth of ~670 km beneath the Java Sea, although a seismic gap exists between 300 and 500 km depth (Hamilton, 1979; Puspito & Shimazaki, 1995; Widiyantoro & Van der Hilst, 1996, 1997). Tomographic imaging reveals a seismic anomaly beneath the Sunda arc that is detected to a depth of at least 1500 km. Beneath Java, the lithospheric slab appears to be continuous and to penetrate into the lower mantle (Puspito & Shimazaki, 1995; Widiyantoro & Van der Hilst, 1996, 1997). The shallow slab dips in a northward direction at a low angle to a depth of ~100 km and at an angle of ~60° below that depth, whereas the deep slab sinks almost vertically into the lower mantle (Hamilton, 1979; Jarrard, 1986; Widiyantoro & Van der Hilst, 1996, 1997).

The Merapi volcanic complex, which is the youngest and southernmost of a volcanic chain extending NNW to Ungaran volcano (Van Bemmelen, 1949) (Fig. 2), is situated ~350 km north of the Java trench. It is located at the western end of the Solo zone (Van Bemmelen, 1949); a longitudinal depression in East–Central Java that consists of Tertiary and older rocks underneath a thick cover of alluvial deposits. Marine limestones are typical of the subvolcanic basement of Merapi

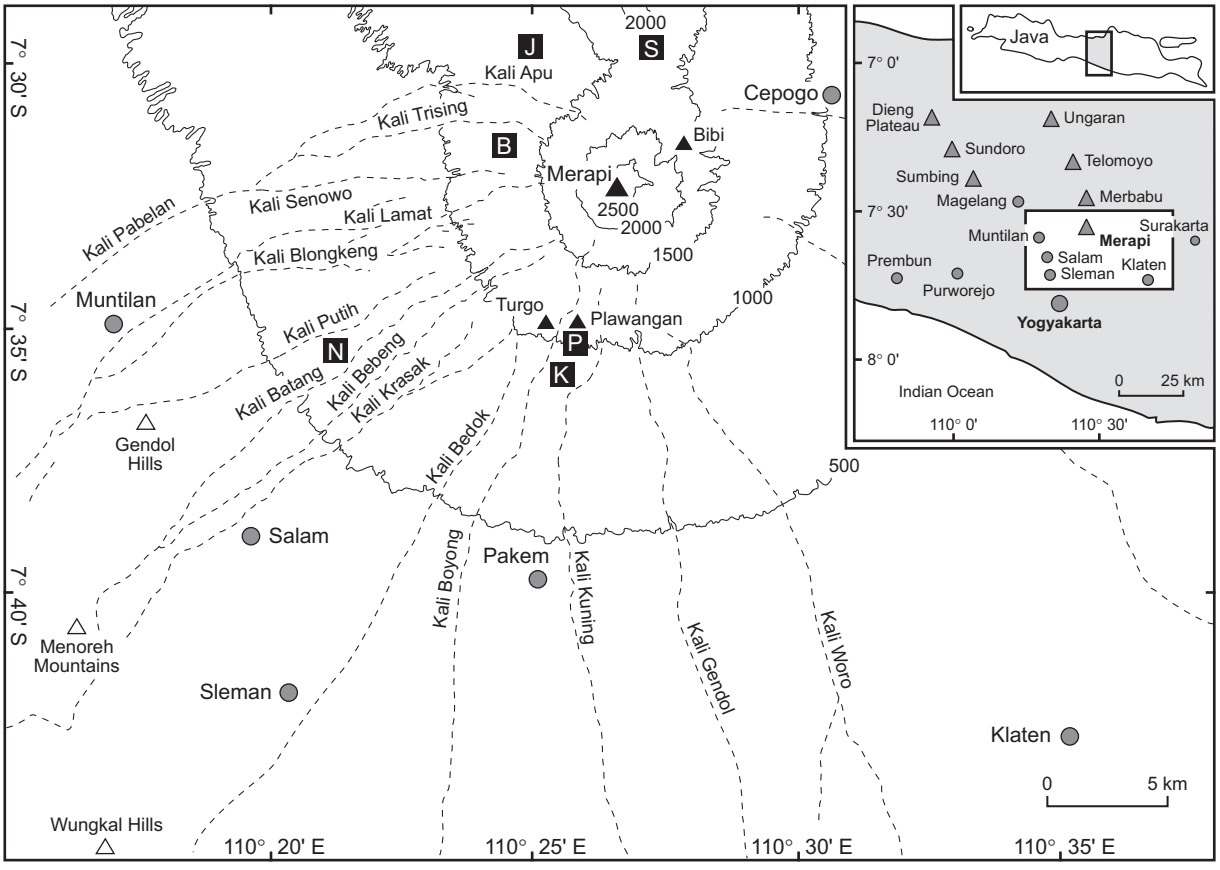

Fig. 2. Topographic sketch map of Merapi volcano in Central Java showing major towns (grey circles) and volcano observation posts (■): K, Kaliurang; P, Plawangan; N, Ngepos; B, Babadan; J, Jrakah; S, Selo. Dashed lines indicate major drainages leading from the volcano. ▲, Merapi summit and a series of hills rising from the volcanic complex; △, hills of the surrounding plain. Contours are in metres. Inset map shows the location of Merapi relative to nearby Quaternary volcanoes (grey triangles) in Central Java.

(Van Bemmelen, 1949), which is further illustrated by the presence of abundant calc-silicate xenoliths in the Merapi volcanics (e.g. Camus *et al*., 2000).

GEOLOGY OF THE MERAPI VOLCANIC COMPLEX

Merapi is a basalt to basaltic andesite volcanic complex of 2911 m height rising above the lowlands north of Yogyakarta in Central Java (Fig. 2). Pyroclastic flows and lahars accompanying growth and collapse of the active summit lava dome of the modern Merapi cone (New Merapi) have devastated populated areas on the southern and western flanks of the volcano and caused many fatalities during recent and historical time (Voight *et al*., 2000). Pyroclastic deposits of Holocene age cover large areas of the volcano's lower flanks (Andreastuti *et al*., 2000; Camus *et al*., 2000; Newhall *et al*., 2000; Gertisser, 2001) and are herein collectively referred to as the Holocene Pyroclastic Series (HPS). These deposits are underlain by a thick sequence of basaltic andesite lavas and intercalated pyroclastic deposits of an eroded older volcanic edifice (Old Merapi) that is now exposed in the deeply dissected northern and eastern flanks of the volcanic complex (Van Bemmelen, 1949; Newhall *et al*., 2000). The horseshoe-shaped morphology of this older edifice suggests the occurrence of one or possibly several flank collapses that left a somma rim high on the volcano's northern and eastern flanks and may have sent one or more debris avalanches down its western slopes (Van Bemmelen, 1949; Berthommier, 1990; Camus *et al*., 2000; Newhall *et al*., 2000). Volcanic construction of the older volcanic edifice may have begun as early as 9630 ± 60 years BP (^{14}C dating: Newhall *et al*., 2000) or even before 11 792 ± 90 years BP (^{14}C dating: Gertisser, 2001). However, volcanism at Merapi certainly began earlier—possibly as early as 40 000 years

BP (Berthommier, 1990; Camus *et al.*, 2000)—with a Proto-Merapi (Newhall *et al.*, 2000) or Ancient Merapi stage (Berthommier, 1990; Camus *et al.*, 2000), whose relics are preserved in the two steep-sided hills of Gunung Turgo and Gunung Plawangan on the southern flank of Merapi (Fig. 2). Ancient Merapi has been interpreted by Berthommier (1990) and Camus *et al.* (2000) to lie on an even older volcanic structure, Gunung Bibi, which is exposed in the northeastern sector of the volcanic complex (Fig. 2). A K–Ar age of 0·67 ± 0·25 Ma for a lava flow from Gunung Bibi (Berthommier, 1990; Camus *et al.*, 2000) supports this hypothesis, although Newhall *et al.* (2000) interpreted Gunung Bibi as a vent of Old Merapi.

SAMPLE SELECTION AND ANALYTICAL TECHNIQUES

The sample suite that forms the basis of this study is representative of the younger eruptive stages of Merapi. It includes (1) the lava sequences of the somma rim, (2) pyroclastic-flow and tephra-fall deposits of the overlying HPS and (3) eruptive products of selected effusive (dome-forming) and pyroclastic flow-forming eruptions of the recent and historical activity of Merapi, which can be traced back to the late 18th century (Voight *et al.*, 2000).

A total of 178 whole-rock samples (Gertisser, 2001) was analysed for major and trace elements by X-ray fluorescence (XRF). A subset of samples was chosen for high-precision trace element analysis by inductively coupled plasma mass spectrometry (ICP-MS), for B analysis by absorption spectrometry, and for radiogenic (Sr, Nd, Pb) and stable (O) isotope determinations. Additional O isotope compositions were determined on plagioclase phenocrysts from some of the same samples. To estimate the isotopic composition of the subvolcanic basement, two Tertiary calcareous sediment samples from the local upper crust and a calc-silicate xenolith found in the Merapi lavas were selected for Sr, Nd, Pb and O isotopic analyses. Analytical results are reported in Tables 1 and 2.

Abundances of major elements (SiO_2, TiO_2, Al_2O_3, Fe_2O_3*, MnO, MgO, CaO, Na_2O, K_2O, P_2O_5) and selected trace elements (Ba, Rb, Sr, Zr, Ni, Cr, Co, V) were determined using a Philips PW 2404 automated XRF spectrometer at the Universität Freiburg. Before analysis, exposed portions and weathered surfaces of the samples were carefully removed and, where possible, fresh interior slabs of lava and pyroclastic samples were processed. Tropical weathering has apparently affected pumiceous clasts from older air-fall deposits, as indicated by elevated loss on ignition (LOI) values. All samples were ground in an agate mill. Major and trace elements were determined on fused discs and pressed powder pellets, respectively. Reproducibility and accuracy for major and minor elements is better than 1% relative. Analytical uncertainty varies from 1 to 10 ppm for trace elements, depending on the element. Accuracy and precision were monitored using several international rock standards. LOI was determined by weight difference at heating to 1050°C for 90 min. LOI, as listed in Table 1, is the total effect of dehydration (loss of weight) and oxidation (gain of weight).

Rare earth elements (REE) and other trace elements were analysed by ICP-MS at the CRPG-CNRS in Nancy (France). Typical analytical precision ranges from ≤5 to ≤10% depending on the concentration of the specific element. Boron concentrations were determined by absorption spectrometry at the same laboratory. The detection limit for the B analysis is 1 ppm. Analytical precision varies with B concentration and ranges from 10 to 15% at the concentrations determined for the Merapi rocks.

All isotopic measurements were made on bulk-rock powders and plagioclase separates without further pretreatment at the Universität Tübingen using analytical methods described in detail by Hegner *et al.* (1995*a*, 1995*b*).

Strontium, neodymium and lead isotopic compositions were determined by thermal ionization mass spectrometry on a Finnigan MAT 262 mass spectrometer. Strontium was loaded with a Ta–Hf activator on pre-conditioned W filaments and was measured in single-filament mode. Nd was loaded as phosphate on pre-conditioned Re filaments and measurements were performed in an Re double-filament configuration. The $^{87}Sr/^{86}Sr$ isotope ratios were normalized to $^{86}Sr/^{88}Sr = 0{\cdot}1194$ and the $^{143}Nd/^{144}Nd$ isotope ratios to $^{146}Nd/^{144}Nd = 0{\cdot}7219$. Measured values of the NBS 987 Sr standard over the period of this study (January–December 2001) were 0·710261 ± 0·000016 (2σ, $n = 29$, reference value = 0·710248). Analyses of the Ames Nd standard within the same period gave a $^{143}Nd/^{144}Nd$ ratio of 0·512119 ± 0·000009 (2σ, $n = 40$, reference value = 0·512130). Pb was loaded with a Si-gel onto a pre-conditioned Re filament and measured at 1250–1300°C in single-filament mode. Total procedure blanks were <50 pg. A factor of 1‰ per mass unit for instrumental mass fractionation was applied to all Pb analyses, using NBS SRM 981 as reference material. The estimated 2σ uncertainty of the reported Pb isotope ratios is better than 0·01%.

Oxygen isotope ratios were measured using a Finnigan MAT 252 gas source mass spectrometer (Hegner *et al.*, 1995*a*). The results are reported as per mil (‰) deviations relative to Standard Mean

Table 1: Major element (wt %), trace element (ppm) and isotopic compositions of the Merapi volcanics

Series:	Merapi medium-K series								
Eruptive stage:	Lava flows, Merapi-Somma					Holocene Pyroclastic Series (HPS)			
Sample:	M95-026	M96-056	M96-071	M98-047	M98-107	M96-073	M96-137	M96-163	M98-0532
Major elements (XRF)									
SiO_2	55·50	55·41	56·60	55·58	55·70	54·50	54·12	51·40	54·39
TiO_2	0·78	0·76	0·73	0·79	0·69	0·86	0·80	0·73	0·82
Al_2O_3	18·33	18·69	18·75	18·45	18·54	18·85	18·77	21·46	18·59
Fe_2O_3*	8·33	8·07	7·51	7·79	7·44	8·28	8·47	7·56	7·87
MnO	0·17	0·18	0·16	0·17	0·15	0·20	0·18	0·17	0·19
MgO	3·41	3·17	2·26	2·56	2·28	2·75	3·17	2·56	2·68
CaO	8·44	8·43	8·01	8·08	8·04	8·50	8·75	7·69	8·28
Na_2O	3·43	3·59	4·00	3·67	3·97	3·77	3·61	3·09	3·81
K_2O	1·71	1·67	1·72	1·88	1·73	1·71	1·61	1·25	1·77
P_2O_5	0·21	0·22	0·24	0·32	0·24	0·28	0·27	0·25	0·27
LOI	0·10	0·29	0·49	1·03	1·14	0·30	0·38	4·24	1·77
Total	100·41	100·47	100·49	100·33	99·90	100·00	100·14	100·40	100·45
Trace elements (XRF)									
Ba	492	458	418	495	479	487	409	402	437
Rb	46	33	40	47	46	46	39	38	43
Sr	488	516	497	506	557	528	530	511	518
Zr	92	100	104	115	112	119	99	107	112
Ni	7	b.d.	3	3	4	b.d.	3	b.d.	3
Cr	15	41	11	13	12	12	57	5	23
Co	21	13	15	17	20	9	17	9	15
V	225	179	135	162	205	183	165	154	177
Trace elements (ICP-MS)[1]									
Ba	451	454	430	434	458	478	445	411	439
Rb	46·1	38·3	42·7	47·7	49·0	42·5	40·6	38·7	44·0
Sr	496	519	519	520	573	532	552	533	547
B		10		12			15		16
Be	1·01	0·81	0·63	1·25	1·13	1·14	0·86	1·15	0·88
Mo	0·82	0·89	0·70	1·12	1·11	0·93	1·12	0·95	1·00
Pb	14·8	15·3	18·3	17·3	15·7	13·0	19·6	15·1	14·7

Series:	Merapi medium-K series								
Eruptive stage:	Lava flows, Merapi-Somma					Holocene Pyroclastic Series (HPS)			
Sample:	M95-026	M96-056	M96-071	M98-047	M98-107	M96-073	M96-137	M96-163	M98-0532
Zr	88	92	102	113	112	107	99	95	115
Nb	2·63	2·95	3·62	4·65	4·62	4·17	3·65	3·38	4·12
Hf	2·01	2·31	2·35	2·64	2·66	2·54	2·45	2·23	2·74
Ta	0·21	0·23	0·30	0·36	0·36	0·34	0·31	0·25	0·31
Th	6·27	5·52	5·87	6·16	6·20	5·92	5·98	5·35	5·07
U	1·31	1·16	1·29	1·53	1·42	1·29	1·28	1·06	1·34
Y	17·9	20·9	20·1	21·1	22·3	24·1	22·3	21·2	24·6
Ni	4·5	2·1	2·0	2·7	5·2	1·6	1·6	1·7	2·8
Cr	11·2	6·2	7·1	5·9	7·2	5·6	5·5	6·2	3·3
Co	21·4	19·1	13·3	17·0	22·2	16·3	18·7	18·3	16·6
V	243	213	150	189	239	200	199	194	197
La	14·4	14·4	15·3	19·2	20·0	16·5	16·1	15·6	16·3
Ce	29·1	28·2	31·7	38·0	41·1	35·3	33·5	31·5	33·6
Pr	3·32	3·43	3·68	4·51	4·91	4·41	4·16	4·00	4·20
Nd	13·7	14·7	15·6	18·7	19·3	17·6	18·0	16·4	18·1
Sm	3·06	3·33	3·58	4·35	4·4	4·22	4·24	3·92	4·12
Eu	1·00	1·19	1·14	1·34	1·42	1·40	1·39	1·18	1·44
Gd	3·03	3·43	3·31	4·03	4·29	4·20	3·89	3·73	4·29
Tb	0·469	0·513	0·476	0·592	0·622	0·624	0·577	0·536	0·615
Dy	2·94	3·14	3·25	3·56	3·85	3·90	3·55	3·25	3·71
Ho	0·544	0·616	0·68	0·737	0·805	0·845	0·749	0·718	0·769
Er	1·59	1·72	1·67	1·94	2·30	2·29	2·18	1·96	2·17
Tm	0·254	0·299	0·262	0·343	0·330	0·382	0·353	0·322	0·358
Yb	1·70	1·87	1·91	2·09	2·10	2·24	2·16	2·00	2·34
Lu	0·281	0·326	0·302	0·325	0·338	0·385	0·349	0·339	0·371
Isotopic ratios									
$^{87}Sr/^{86}Sr$	0·705260 ± 11	0·705275 ± 11		0·705014 ± 09	0·705169 ± 10	0·705392 ± 11	0·705277 ± 11	0·705155 ± 10	0·705353 ± 10
$^{143}Nd/^{144}Nd$	0·512727 ± 09	0·512765 ± 10		0·512712 ± 09	0·512722 ± 10	0·512774 ± 09	0·512758 ± 07	0·512754 ± 08	0·512759 ± 10
$^{206}Pb/^{204}Pb$	18·784	18·771		18·740	18·781	18·757	18·727		
$^{207}Pb/^{204}Pb$	15·716	15·709		15·689	15·715	15·695	15·681		
$^{208}Pb/^{204}Pb$	39·208	39·170		39·110	39·215	39·138	39·015		
$\delta^{18}O$ w.r. (‰)	+6·4	+6·6		+6·9	+6·9	+6·3	+6·8	+8·3	+7·3
$\delta^{18}O$ pl. (‰)							+6·5	+7·0	

Table 1: Continued

Series:	Merapi high-K series								
Eruptive stage:	Holocene Pyroclastic Series (HPS)								
Sample:	M96-075	M96-102	M96-164	M96-167	M97-021	M97-031	M97-0392	M97-053	M97-077
Major elements (XRF)									
SiO_2	53·87	51·87	51·86	54·41	52·85	55·62	52·86	54·12	52·45
TiO_2	0·71	0·81	0·84	0·75	0·88	0·71	0·87	0·74	0·78
Al_2O_3	18·87	20·44	19·31	18·72	18·57	18·63	18·80	18·92	18·96
Fe_2O_3*	8·13	8·24	8·48	8·31	9·09	7·37	8·78	8·19	8·89
MnO	0·19	0·20	0·20	0·18	0·18	0·19	0·19	0·19	0·20
MgO	3·03	2·47	3·02	2·94	3·51	2·37	3·20	2·91	3·27
CaO	8·55	8·86	9·30	8·39	9·41	7·79	8·94	8·49	9·18
Na_2O	3·43	3·35	3·36	3·57	3·36	3·80	3·48	3·47	3·32
K_2O	2·04	1·74	1·82	2·30	1·98	2·38	2·14	2·15	1·91
P_2O_5	0·29	0·31	0·29	0·27	0·25	0·25	0·24	0·30	0·31
LOI	1·06	1·63	1·46	0·16	0·42	1·34	0·55	1·08	0·91
Total	100·17	99·91	99·93	99·98	100·49	100·45	100·05	100·56	100·18
Trace elements (XRF)									
Ba	484	455	476	561	488	604	498	544	455
Rb	49	47	48	57	49	67	55	60	43
Sr	562	594	582	563	514	593	543	585	586
Zr	99	103	97	91	83	105	86	94	98
Ni	b.d.	b.d.	b.d.	2	5	b.d.	2	2	3
Cr	28	11	20	17	79	15	26	25	67
Co	15	13	14	16	19	9	13	6	16
V	168	182	200	194	223	132	211	170	189
Trace elements (ICP-MS)									
Ba	525		477	533	531	602	515	512	457
Rb	50·3		45·2	58·1	49·4	64·5	48·7	52·7	44·1
Sr	570		611	600	555	614	569	586	588
B						19	20		
Be	1·03		1·13	1·04	0·77	1·24	0·93	1·29	0·83
Mo	1·14		1·04	1·16	0·83	1·26	1·19	0·97	0·92
Pb	19·6		18·9	15·7	24·3	13·8	18·2	17·6	16·7

Series:	Merapi high-K series								
Eruptive stage:	Holocene Pyroclastic Series (HPS)								
Sample:	M96-075	M96-102	M96-164	M96-167	M97-021	M97-031	M97-0392	M97-053	M97-077
Zr	90		90	89	83	99	85	88	89
Nb	3·31		2·92	2·77	2·85	3·27	2·73	2·85	3·18
Hf	2·23		2·21	2·13	2·06	2·45	2·12	2·01	2·17
Ta	0·27		0·22	0·20	0·21	0·25	0·20	0·21	0·22
Th	7·61		7·33	6·91	6·56	8·91	6·68	6·86	6·94
U	1·57		1·35	1·44	1·37	1·71	1·49	1·22	1·22
Y	22·1		23·4	22·7	22·5	22·3	22·4	22·6	22·5
Ni	2·3		3·3	2·3	4·6	3·0	2·9	1·4	0·1
Cr	9·2		24·5	8·3	12·6	9·2	8·9	6·6	5·7
Co	17·1		18·9	20·0	23·6	16·9	21·9	18·8	19·2
V	193		224	229	249	186	272	207	205
La	18·7		18·0	18·7	16·8	20·3	15·6	18·4	17·9
Ce	38·0		36·0	36·2	33·1	40·4	31·6	36·2	35·7
Pr	4·38		4·53	4·08	4·07	4·74	3·91	4·40	4·27
Nd	18·1		18·9	17·1	17·0	18·6	16·2	16·8	18·3
Sm	4·01		4·68	3·93	4·17	4·40	4·15	4·19	4·27
Eu	1·33		1·35	1·14	1·31	1·37	1·31	1·27	1·30
Gd	3·85		4·17	3·36	3·58	3·49	3·37	3·70	3·69
Tb	0·584		0·600	0·519	0·568	0·526	0·606	0·570	0·581
Dy	3·62		3·86	3·26	3·56	3·54	3·41	3·30	3·54
Ho	0·780		0·791	0·678	0·741	0·767	0·701	0·722	0·739
Er	2·15		2·14	1·95	1·92	2·00	2·01	1·98	2·08
Tm	0·345		0·341	0·304	0·322	0·319	0·358	0·282	0·337
Yb	2·12		2·06	1·93	2·02	2·17	2·10	1·99	2·01
Lu	0·358		0·358	0·326	0·312	0·352	0·345	0·325	0·339
Isotopic ratios									
$^{87}Sr/^{86}Sr$		0·705536 ± 09		0·705625 ± 11	0·705741 ± 11	0·705696 ± 10	0·705663 ± 10	0·705658 ± 10	
$^{143}Nd/^{144}Nd$		0·512742 ± 09		0·512711 ± 09	0·512712 ± 09	0·512701 ± 10	0·512714 ± 11	0·512678 ± 09	
$^{206}Pb/^{204}Pb$				18·760	18·769	18·766	18·763		
$^{207}Pb/^{204}Pb$				15·678	15·685	15·684	15·688		
$^{208}Pb/^{204}Pb$				39·098	39·125	39·117	39·130		
$\delta^{18}O$ w.r. (‰)		+6·9		+6·0	+6·7	+7·0	+6·2	+7·0	
$\delta^{18}O$ pl. (‰)		+6·7						+6·8	

Table 1: Continued

Series:	Merapi high-K series							
Eruptive stage:	Holocene Pyroclastic Series (HPS)					Recent and historical eruptive products		
Sample:	M97-0781	M98-030	M98-031	M98-066	M98-096	M95-011	M96-142	M97-068
Major elements (XRF)								
SiO_2	53·24	52·13	51·70	53·06	53·29	52·88	55·88	51·85
TiO_2	0·75	0·78	0·84	0·81	0·78	0·80	0·69	0·87
Al_2O_3	19·35	19·02	18·77	18·97	18·64	18·61	19·05	18·53
Fe_2O_3*	8·31	8·49	8·38	8·95	8·55	9·32	7·45	9·65
MnO	0·20	0·20	0·20	0·20	0·20	0·20	0·18	0·21
MgO	2·82	2·80	3·09	3·23	3·22	3·50	2·44	3·90
CaO	8·88	8·72	9·23	9·23	8·86	9·39	8·13	9·58
Na_2O	3·43	3·39	3·35	3·41	3·45	3·30	3·76	3·20
K_2O	2·03	1·99	1·90	2·05	2·05	2·00	2·25	1·98
P_2O_5	0·32	0·31	0·26	0·30	0·29	0·29	0·31	0·29
LOI	0·73	2·07	2·49	0·27	0·81	0·07	0·24	0·31
Total	100·05	99·90	100·21	100·48	100·14	100·35	100·37	100·36
Trace elements (XRF)								
Ba	509	580	534	506	473	445	539	425
Rb	56	52	52	51	51	47	53	46
Sr	581	591	575	557	583	573	563	560
Zr	100	100	94	90	98	93	113	90
Ni	b.d.	3	2	3	b.d.	b.d.	b.d.	2
Cr	10	10	18	15	14	23	42	23
Co	11	18	14	18	15	18	9	25
V	167	187	193	203	171	183	130	209
Trace elements (ICP-MS)								
Ba	486			506	535	439	522	431
Rb	48·0			47·4	50·8	46·8	52·4	45·7
Sr	624			565	584	600	546	603
B				19		17	17	17
Be	0·71			0·89	1·12	0·93	0·98	1·13
Mo	0·98			1·05	1·03	1·05	1·22	0·92
Pb	19·6			18·5	18·9	15·7	19·8	14·8
Zr	94			87	91	86	107	83
Nb	3·55			3·10	3·25	3·30	4·06	2·94

Series:	Merapi high-K series							
Eruptive stage:	Holocene Pyroclastic Series (HPS)					Recent and historical eruptive products		
Sample:	M97-0781	M98-030	M98-031	M98-066	M98-096	M95-011	M96-142	M97-068
Hf	2·58			2·24	2·32	2·15	2·74	2·14
Ta	0·26			0·24	0·25	0·23	0·34	0·21
Th	8·26			6·77	6·68	7·23	8·04	6·16
U	1·56			1·51	1·46	1·29	1·43	1·02
Y	23·3			22·1	22·3	23·0	23·9	22·8
Ni	0·1			3·1	4·1	3·1	0·8	2·6
Cr	6·0			4·9	9·7	11·7	8·2	16·0
Co	18·8			20·4	19·8	21·6	14·2	27·8
V	206			220	211	222	156	249
La	18·8			18·4	19·0	17·2	20·2	17·3
Ce	38·6			36·4	36·5	34·5	39·0	34·6
Pr	4·63			4·24	4·37	4·18	4·79	4·28
Nd	19·1			18·8	19·1	17·8	19·9	18·0
Sm	4·70			4·37	4·27	4·34	4·57	4·33
Eu	1·31			1·37	1·40	1·34	1·38	1·36
Gd	3·84			3·96	4·00	4·13	4·20	3·65
Tb	0·615			0·595	0·636	0·588	0·622	0·627
Dy	3·68			3·77	4·07	3·46	3·88	3·45
Ho	0·785			0·732	0·747	0·708	0·837	0·724
Er	2·13			2·12	2·21	2·11	2·32	1·93
Tm	0·348			0·361	0·340	0·314	0·386	0·318
Yb	2·10			2·16	2·12	2·22	2·35	2·01
Lu	0·360			0·323	0·338	0·325	0·379	0·330
Isotopic ratios								
$^{87}Sr/^{86}Sr$		0·705725 ± 10	0·705561 ± 09	0·705826 ± 09	0·705643 ± 10		0·705737 ± 11	0·705711 ± 11
$^{143}Nd/^{144}Nd$		0·512721 ± 06	0·512735 ± 09	0·512675 ± 10	0·512686 ± 10		0·512723 ± 10	0·512671 ± 09
$^{206}Pb/^{204}Pb$				18·780	18·775		18·773	18·727
$^{207}Pb/^{204}Pb$				15·699	15·702		15·714	15·671
$^{208}Pb/^{204}Pb$				39·175	39·178		39·195	39·038
$\delta^{18}O$ w.r. (‰)		+7·1	+7·5	+6·6	+6·5		+6·7	+6·3
$\delta^{18}O$ pl. (‰)		+6·6	+6·6					

[1]Boron analyses by absorption spectrometry.
$\delta^{18}O$ values are reported in ‰ relative to SMOW. $\delta^{18}O$ analyses were obtained for whole-rock samples (w.r.) and plagioclase separates (pl.). Fe_2O_3*, total Fe as Fe_2O_3; LOI, loss on ignition; b.d., below detection limit.

Table 2: Isotopic compositions of selected crustal rocks of Java

Sample	$^{87}Sr/^{86}Sr$	$^{143}Nd/^{144}Nd$	$^{206}Pb/^{204}Pb$	$^{207}Pb/^{204}Pb$	$^{208}Pb/^{204}Pb$	$\delta^{18}O$ (‰ SMOW)
Crustal xenolith (calc-silicate)						
MX-6	0·706507 ± 09	0·512154 ± 09	19·728	15·750	41·440	+11·5
Calcareous sediments (local upper crust)						
MX99-1	0·707350 ± 09	0·512564 ± 09	18·989	15·660	39·865	+20·5
MX99-2	0·706932 ± 09	0·512749 ± 10	18·720	15·637	39·209	+18·9

Ocean Water (SMOW) and refer to a certified value of 9·6 ± 0·1% measured on NBS 28. For the O isotope determinations at least two measurements were performed for a given sample and the average $\delta^{18}O$ values are reported in Table 1. All values were reproduced within an analytical error of 0·1–0·2‰.

PETROGRAPHY AND MINERAL CHEMISTRY

This section briefly describes the petrography of the Merapi medium-K and high-K series rocks and summarizes the compositions of the major mineral phases from selected samples of both series, as determined by electron microprobe. Analytical techniques and the complete dataset have been given by Gertisser (2001).

The basalts and basaltic andesites of the medium-K and high-K series of Merapi display similar petrographic characteristics that reflect the overall restricted range of whole-rock compositions. Typical mineral assemblages in the mafic rock types consist of plagioclase, clinopyroxene, rare olivine and titanomagnetite. Some samples also contain phenocrysts of amphibole. The major phenocryst phases in the more evolved compositions include plagioclase, clinopyroxene, orthopyroxene, titanomagnetite and often amphibole. Apatite is a common accessory mineral in the Merapi lavas and occurs as microphenocrysts or inclusions in plagioclase and pyroxene crystals.

The Merapi rocks are generally highly porphyritic with phenocryst contents up to 50–60% of the total rock volume. Phenocrysts, microphenocrysts and mineral aggregates are enclosed within a glassy or fine-grained groundmass that consists of plagioclase, clinopyroxene and titanomagnetite. Plagioclase and Ca-rich clinopyroxene are ubiquitous in the Merapi rocks and dominate the phenocryst assemblage. Plagioclase is by far the most abundant phenocryst phase, followed by clinopyroxene, a characteristic feature of many arc volcanic rocks (Gill, 1981).

Plagioclase crystals can be euhedral, rounded, broken or twinned and are often sieve-textured. Zoning can be normal, reverse or oscillatory. Plagioclase compositions in the Merapi volcanics range from An 30 to An 95. In many cases, the geochemical variations within individual samples or even within single crystals are as large as the total range of variation of plagioclase compositions. The orthoclase content of the plagioclase phenocrysts increases systematically as the anorthite content decreases and reaches maximum values of 8 mol % in the most sodic compositions. The volcanic rocks of the high-K series are characterized by slightly higher orthoclase contents at a given anorthite content compared with the medium-K series rocks.

Clinopyroxene phenocrysts are typically euhedral to subhedral and unzoned or only weakly zoned. In a few samples, clinopyroxene can be found as overgrowth rims on earlier formed orthopyroxene crystals. The clinopyroxene phenocrysts of Merapi are augites, with a few compositions extending into the diopside field (Morimoto, 1988). They span a restricted compositional range (Wo 39–47, En 37–47 and Fs 7–19) typical of clinopyroxenes from arc volcanic rocks (Gill, 1981). Elevated Wo contents (>44 mol %) are limited to the high-K series rocks and appear to be directly related to the K-enriched character of the high-K magmas.

Unzoned or slightly normally zoned olivine phenocrysts and microphenocrysts with forsterite contents ranging from 60 to 80 mol % are present in trace amounts in the more mafic rock types of the two series. In a few cases, microphenocrysts of olivine and orthopyroxene coexist in rocks with 52–54 wt % SiO_2. In more evolved rock types orthopyroxene replaces olivine as a phenocryst phase. Orthopyroxene crystals are fairly homogeneous in composition (En 62–71, Fs 26–35, Wo 2–4) and may be classified as enstatite (Morimoto, 1988).

In the Merapi rocks, amphibole may occur as an accessory, minor or major phenocryst phase, often surrounded by reaction rims composed of small plagioclase, pyroxene and Fe–Ti oxide crystals. Merapi

amphiboles display a narrow range of compositions and are classified as Mg-hastingsite or pargasite (Leake *et al.*, 1997), depending on the assumed ferric iron content.

Titanomagnetite is always present in moderate amounts in the basaltic andesites, whereas it is rare in the basalts. The ulvöspinel contents vary from 20 to 40 mol %.

GEOCHEMISTRY

Major element geochemistry

Representative major and trace element data for Merapi are listed in Table 1. Variations in K_2O content (Fig. 3) clearly divide the eruptive products of Merapi into a medium-K series and a high-K series (Le Maitre *et al.*, 2002), which are characterized by K_{55} (K_2O at 55 wt % SiO_2) values of 1·67 and 2·14, respectively. Some of the lowest K_2O contents can be found in highly altered and hydrated pumiceous clasts, which suggests that K is leached from the glassy groundmass of these samples by low-temperature alteration processes. It is worth mentioning, however, that the high degree of alkali mobility during the hydration process does not affect the geochemical affinity of these rocks, which may still be classified as medium-K (Gertisser, 2001). New stratigraphic and chronological data (Gertisser, 2001; Gertisser & Keller, 2003) suggest that the K_2O abundance at a given SiO_2 content varies with time at Merapi. The lavas from the somma rim and the older HPS deposits display the lowest K_2O contents and define the Merapi medium-K series, whereas the pyroclastic sequences younger than ~1900 ^{14}C years BP, including those from historical and recent eruptions, are distinctly more potassic and therefore are designated as the Merapi high-K series.

Compared with the wide range in K_2O content, Merapi lavas and pyroclastics comprise a rather narrow SiO_2 variation between 48·3 and 57·3 wt % (normalized, on a volatile-free basis). In terms of Al_2O_3 (>18 wt %) and TiO_2 (<1·2 wt %) contents, the Merapi volcanics have chemical characteristics typical of subduction-related volcanic rocks (Gill, 1981).

Variation diagrams of major elements vs SiO_2 are illustrated in Fig. 4. In general, the medium-K and high-K series rocks do not display any significant differences in major element oxides other than K_2O. Within the two magmatic series, TiO_2, Fe_2O_3*, MgO and CaO abundances decrease systematically with increasing silica content, whereas Na_2O and K_2O (Fig. 3) increase. The Al_2O_3 content of the rocks always exceeds 18 wt % and is scattered without any systematic correlation with SiO_2. Extremely high Al_2O_3 contents (>21 wt %) occur only in highly altered samples with >2·5 wt % LOI.

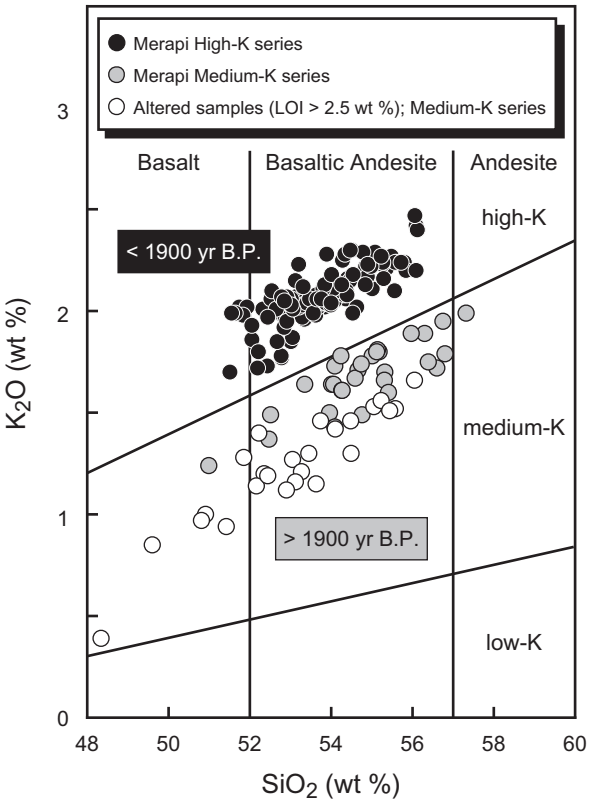

Fig. 3. K_2O vs SiO_2 classification diagram (Le Maitre *et al.*, 2002) for Merapi volcanics. Data points include samples from selected lava flows from the somma rim, pyroclastic-flow and fallout deposits from the overlying Holocene Pyroclastic Series (HPS) as well as dome components and clasts from pyroclastic-flow deposits of the recent and historical activity of Merapi. Lavas from the somma rim and HPS deposits older than ~1900 ^{14}C years BP are medium-K; all younger eruptive products are high-K (Gertisser, 2001; Gertisser & Keller, 2003). ○, Pumiceous clasts, which may have lost K through low-temperature alteration and hydration by meteoric water. All analyses are recalculated to 100 wt % on a volatile-free basis.

Trace element geochemistry

Variations of selected trace elements with SiO_2 are shown in Fig. 5. Although the trace element arrays are generally more scattered than the major element data, systematic variations with SiO_2 are observed. Abundances of incompatible trace elements, such as Rb and Ba, increase systematically with increasing SiO_2 content and the variation of these elements mirrors that of K_2O. In accordance with most incompatible trace elements, Zr tends to increase with increasing SiO_2 content. Vanadium and Co abundances are negatively correlated with SiO_2. Variation of Cr mirrors that of Ni, whose concentrations are generally very low (Table 1). In the SiO_2 variation diagram (Fig. 5), Cr displays a curved trend of strongly decreasing abundance in the mafic compositions and

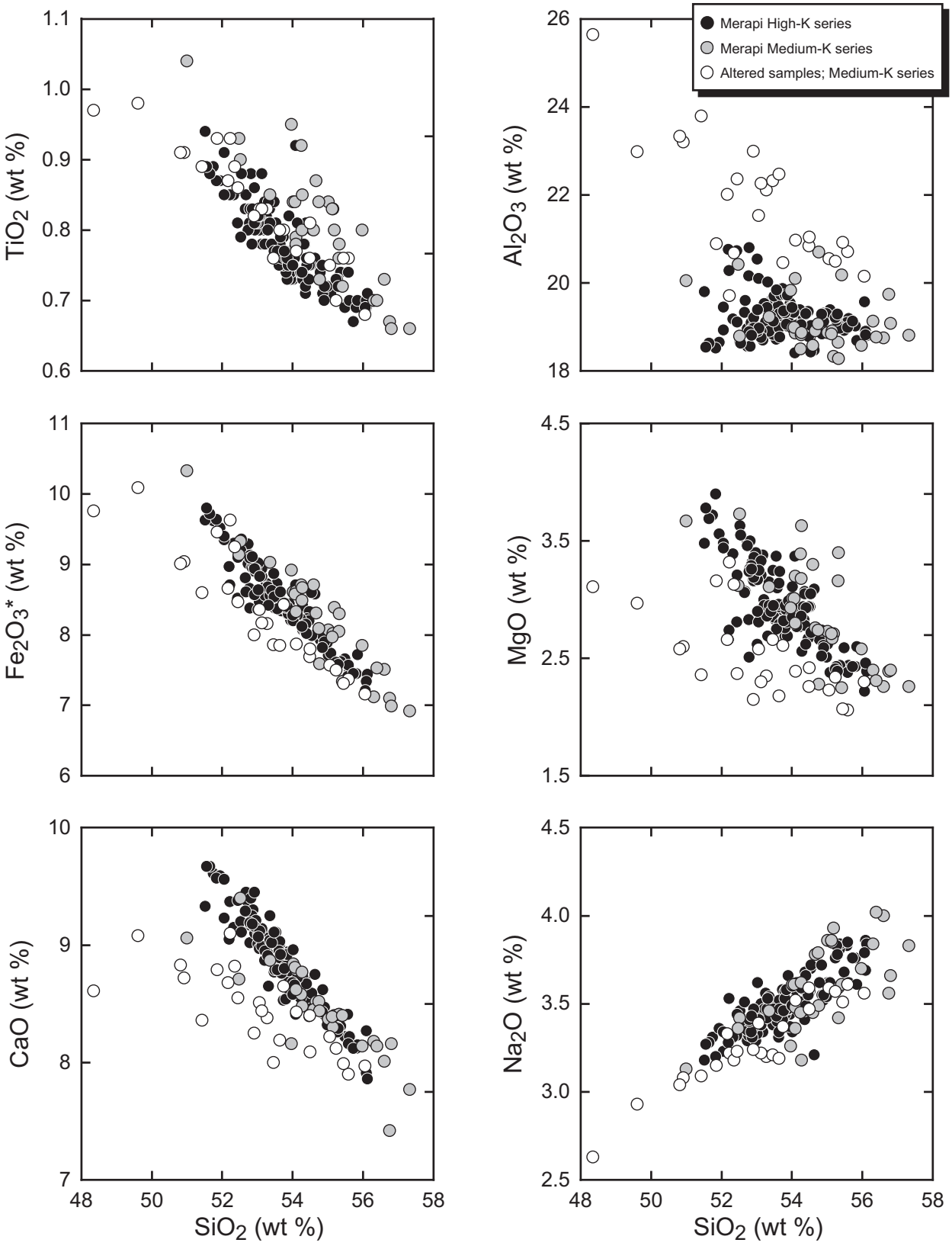

Fig. 4. Variation diagrams for TiO_2, Al_2O_3, Fe_2O_3*, MgO, CaO and Na_2O (wt %) vs SiO_2 (wt %).

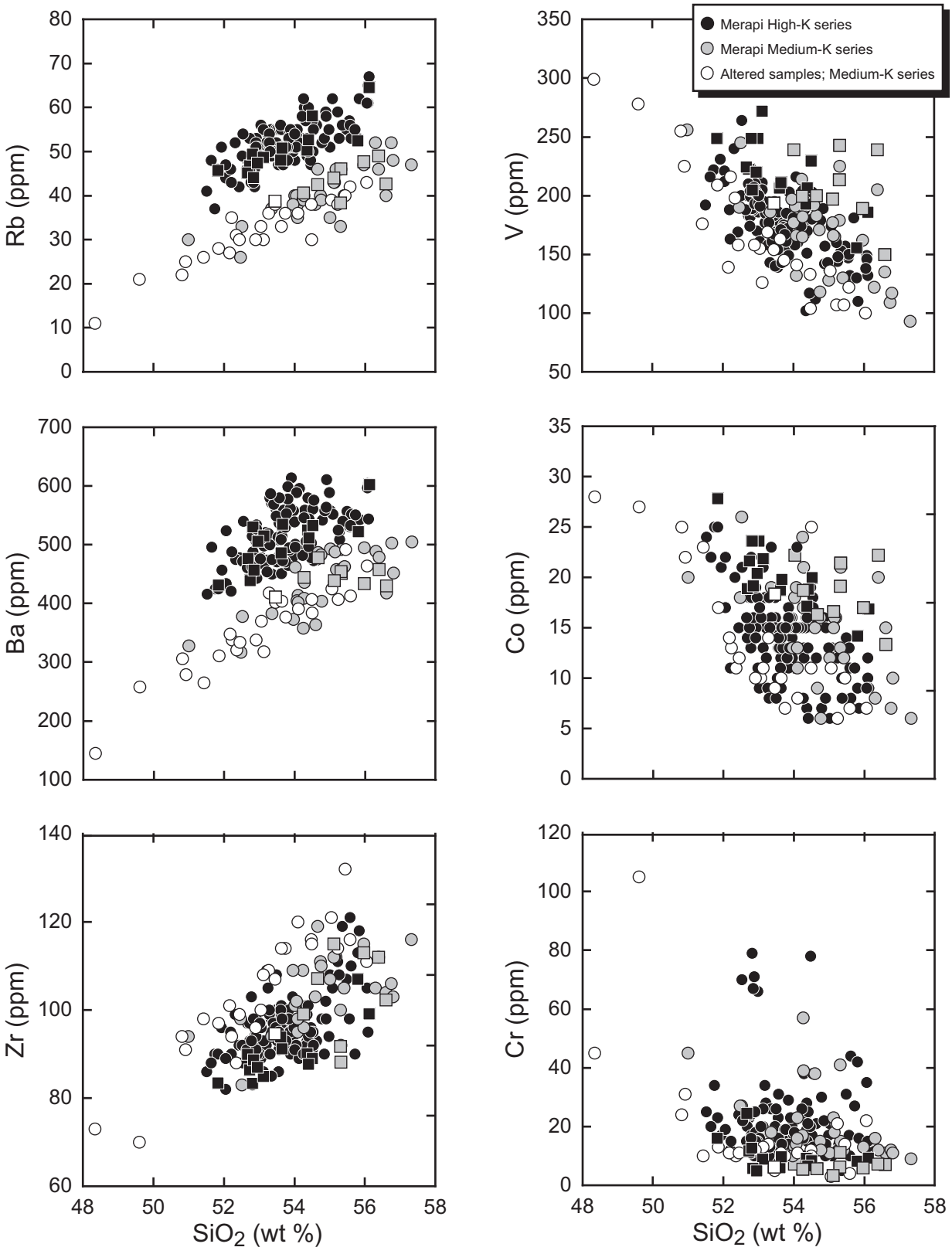

Fig. 5. Variation diagrams for Rb, Ba, Zr, V, Co and Cr (ppm) determined by XRF vs SiO_2 (wt %). Squares denote trace element compositions obtained by ICP-MS.

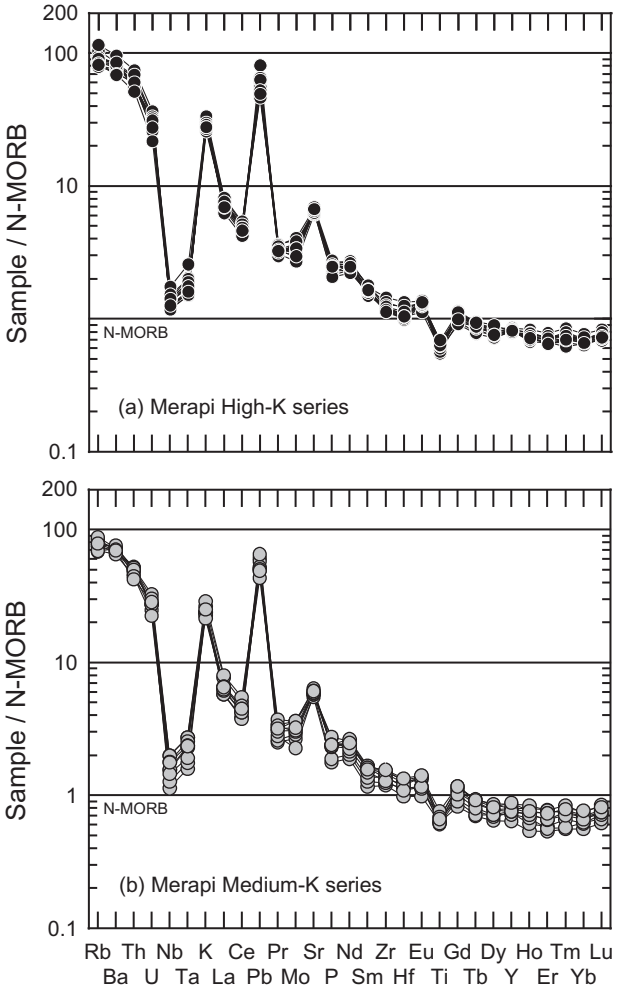

Fig. 6. N-MORB-normalized trace element patterns for (a) high-K and (b) medium-K series rocks of Merapi. Normalizing values from Sun & McDonough (1989).

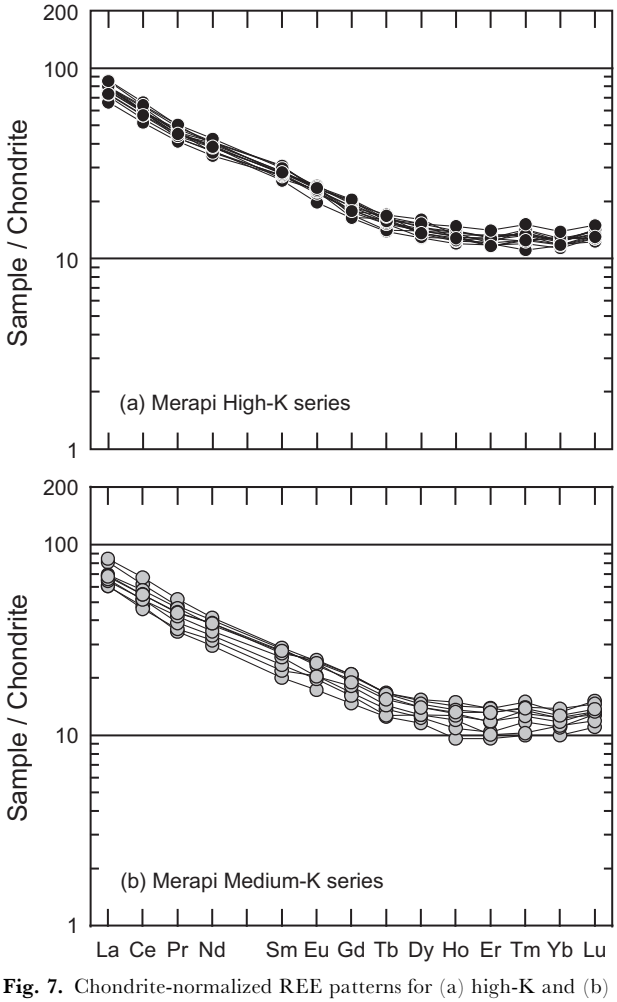

Fig. 7. Chondrite-normalized REE patterns for (a) high-K and (b) medium-K series rocks of Merapi. Normalizing values from Sun & McDonough (1989).

rather constant Cr contents in the more evolved rock types. Additionally, a few samples of intermediate composition display anomalously high Cr contents and follow a linear trend of decreasing Cr abundances with increasing SiO_2 contents. Strontium abundances (Table 1) do not display any systematic variation with SiO_2.

The trace element patterns of the Merapi medium-K and high-K series volcanics normalized to N-MORB (Sun & McDonough, 1989) have a shape that is typical of magmas from subduction-related tectonic settings with enrichment in large ion lithophile elements (LILE), U, Th and Pb and to a lesser extent in light REE (LREE) relative to the heavy REE (HREE) and high field strength elements (HFSE), such as Zr, Hf, Nb, Ta and Ti. Elements such as Nb, Ta and Ti form distinct negative anomalies in the trace element patterns (Fig. 6). In all Merapi volcanics, the HREE are slightly depleted relative to N-MORB.

Chondrite-normalized REE concentrations of the medium-K and high-K series rocks are illustrated in Fig. 7. All Merapi rocks are characterized by fractionated LREE and flat HREE patterns—as is typically found in subduction-related volcanic rocks—but lack significant Eu anomalies. LREE enrichment ranges from 60 to 90 times that of chondrites, whereas chondrite-normalized La/Yb ratios vary from 5·0 to 7·0. Middle REE (MREE) and HREE exhibit relatively flat patterns (Gd_N/Yb_N = 1·3–1·7), generally within the range of 10–15 times chondritic values.

The relatively small compositional differences between the two magmatic series and the effects of fractional crystallization on trace element abundances largely prevent variations in trace element concentrations being detected in N-MORB or chondrite-normalized

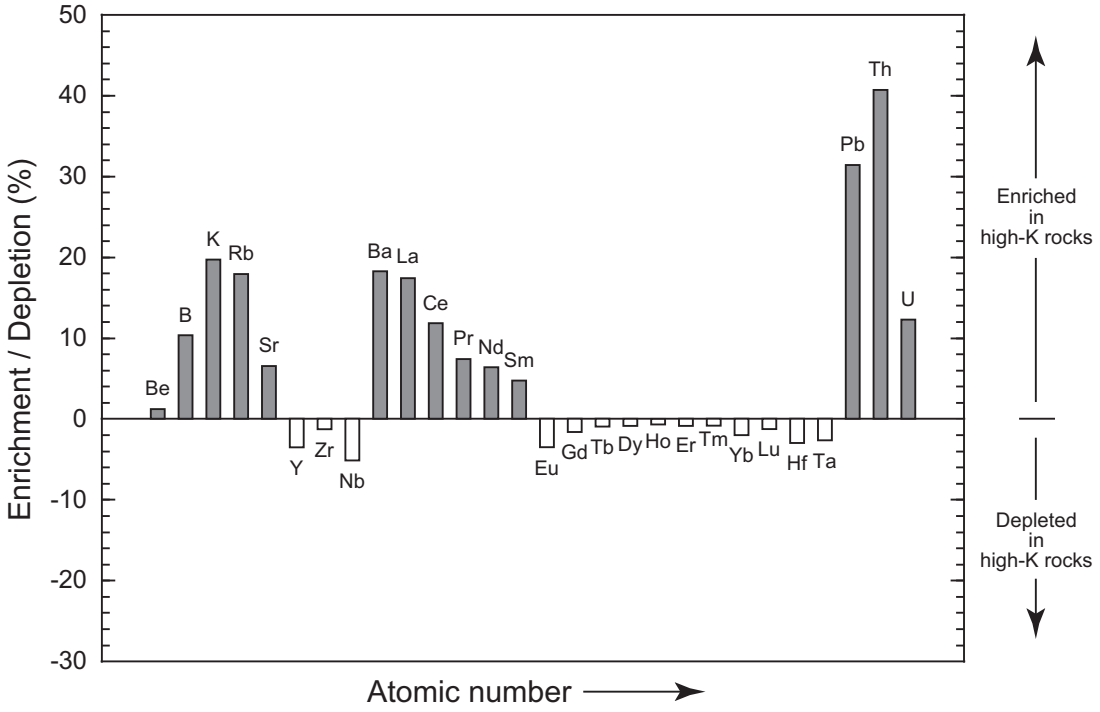

Fig. 8. Percent enrichment or depletion of selected trace elements in the high-K series relative to the medium-K series rocks. Element concentrations used in the calculations were those at 55 wt % SiO_2 as determined by linear extrapolation.

trace element plots (Figs 6 and 7). Therefore, the comparison between the trace element abundances of the medium-K and high-K series rocks has been examined further using rocks characterized by the same degree of differentiation, as summarized in Fig. 8. Relative to the medium-K series rocks, the high-K series volcanics exhibit higher concentrations of fluid-mobile elements, such as B, K, Rb, Sr, Ba, Pb and U, and elevated abundances in LREE (La, Ce, Pr, Nd, Sm) at a fixed SiO_2 content. Thorium, an element generally considered to be much less readily transported in an aqueous fluid phase (Tatsumi *et al.*, 1986; Brenan *et al.*, 1995*a*, 1995*b*; Keppler, 1996), is also enriched in the high-K series relative to the medium-K series rocks. In contrast, concentrations of the MREE, HREE (including Y) and HFSE, such as Zr, Hf, Nb and Ta, are similar or slightly lower in the high-K series compared with the medium-K series volcanics.

Isotope geochemistry

Sr, Nd and Pb isotope data

The $^{87}Sr/^{86}Sr$ ratios of the Merapi volcanics display significant variations between 0·70501 and 0·70583 (Table 1). Previously published Sr isotope ratios for Merapi indicate a similar range from 0·70498 to 0·70594 (Whitford, 1975*a*, 1975*b*; Whitford *et al.*, 1981; Del Marmol, 1989; McDermott & Hawkesworth, 1991; Turner & Foden, 2001). $^{143}Nd/^{144}Nd$ ratios range from 0·51267 to 0·51277 (Table 1) and show a broad negative correlation with $^{87}Sr/^{86}Sr$ ratio (Fig. 9). Systematic variations in the Sr and Nd isotopic ratios at Merapi are most pronounced between the two magmatic series. In general, the high-K series rocks have the highest $^{87}Sr/^{86}Sr$ ratios and the lowest $^{143}Nd/^{144}Nd$ ratios, except for some lavas of medium-K composition from the somma rim that are also characterized by comparatively low $^{143}Nd/^{144}Nd$ ratios within the range of the high-K series rocks (Table 1). Strontium isotopic ratios in the Merapi high-K series range from 0·70554 to 0·70583 and contrast significantly with those in the medium-K series that vary between 0·70501 and 0·70539. The observed compositional gap in Sr isotope ratios between the two magmatic series at Merapi coincides with the transition from the normal to the anomalous calc-alkaline association of the Sunda arc (Whitford, 1975*b*).

In the $^{143}Nd/^{144}Nd$ vs $^{87}Sr/^{86}Sr$ diagram (Fig. 9a), the Merapi rocks define an elongate array well below the field for MORB. The Merapi data plot between the field for MORB and sediments from the Indian Ocean and partly overlap the field of Indian Ocean OIB. In terms of $^{87}Sr/^{86}Sr$ and $^{143}Nd/^{144}Nd$, the Merapi

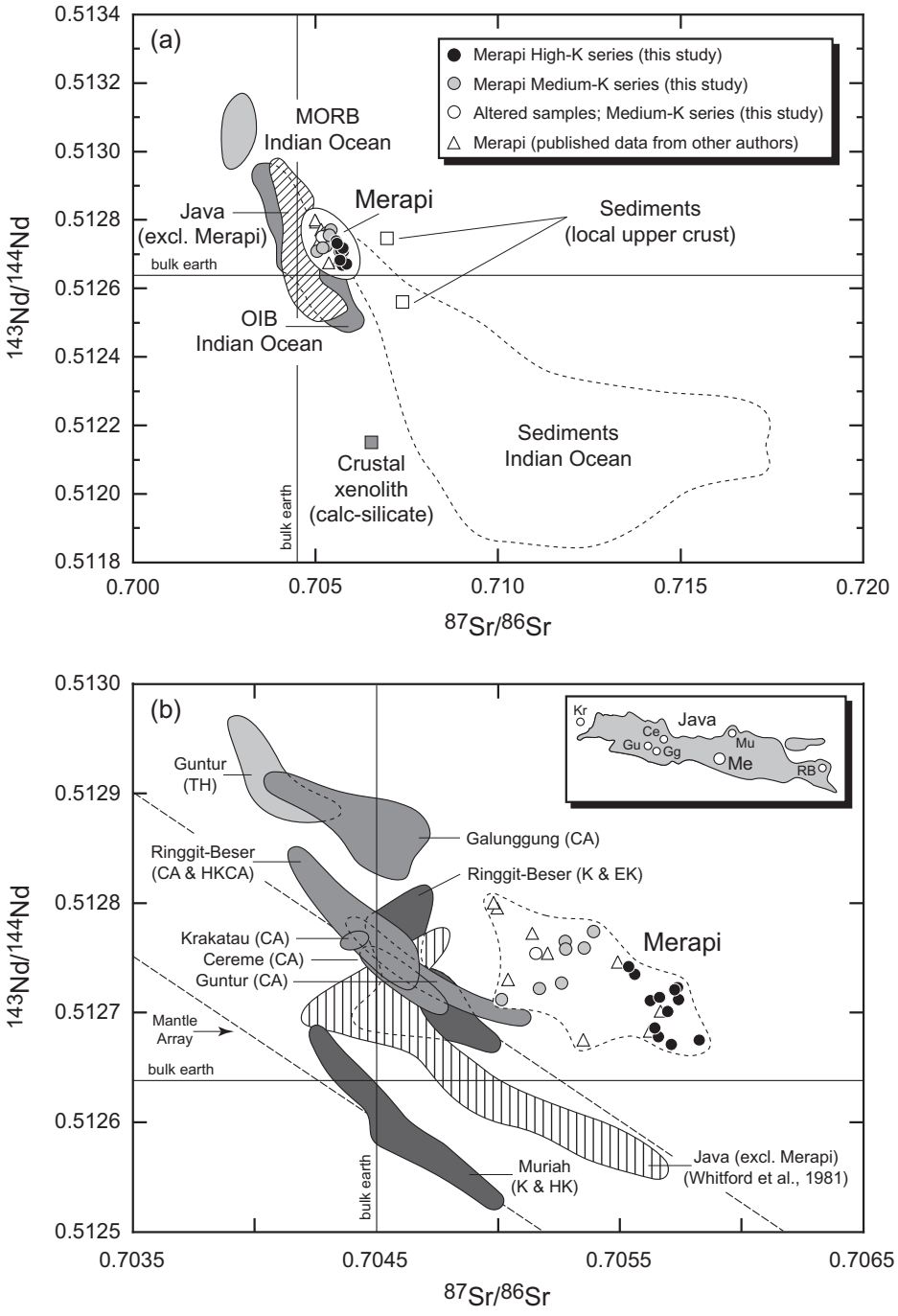

Fig. 9. (a) $^{143}Nd/^{144}Nd$ vs $^{87}Sr/^{86}Sr$ diagram showing data from Merapi in relation to MORB and OIB (St. Paul, Mascarene Islands, Kerguelen, Heard Island) from the Indian Ocean, volcanic rocks from Java (excluding Merapi) and marine sediments from the Indian Ocean. Analyses of a crustal xenolith found in the Merapi lavas and sediments from the local upper crust (Table 2) are shown for comparison. Data sources: MORB, Indian Ocean (Hamelin & Allègre, 1985; Ito *et al*., 1987; Rehkämper & Hofmann, 1997); OIB, Indian Ocean (White & Hofmann, 1982; Hamelin *et al*., 1985; Dosso *et al*., 1988; Barling & Goldstein, 1990; Yang *et al*., 1998); Java (Whitford *et al*., 1981; Edwards *et al*., 1991, 1993; Gerbe *et al*., 1992; Turner & Foden, 2001); marine sediments, Indian Ocean (Ben Othman *et al*., 1989; Gasparon & Varne, 1998); published data, Merapi (Whitford *et al*., 1981; White & Patchett, 1984; Del Marmol, 1989; Turner & Foden, 2001). (b) Close-up of the $^{143}Nd/^{144}Nd$ vs $^{87}Sr/^{86}Sr$ diagram showing data from Merapi relative to other Javanese volcanoes and the mantle array. Volcanic rock series: TH, tholeiitic; CA, calc-alkaline; HKCA, high-K calc-alkaline; K, potassic; EK, enriched potassic; HK, highly potassic. The Java field, defined by Whitford *et al*. (1981), includes calc-alkaline, high-K calc-alkaline and alkaline lavas from several Javanese volcanoes (excluding Merapi). Data sources: Muriah (Mu) (Edwards *et al*., 1991); Galunggung (Gg) (Gerbe *et al*., 1992; Turner & Foden, 2001); Guntur (Gu), Cereme (Ce), Ringgit–Beser (RB) (Edwards *et al*., 1993); Krakatau (Kr) (Turner & Foden, 2001).

volcanics display a rather restricted compositional range displaced from the mantle array—defined by a line passing through average MORB and Bulk Earth values—towards more radiogenic $^{87}Sr/^{86}Sr$ ratios. A close-up of the $^{143}Nd/^{144}Nd$ vs $^{87}Sr/^{86}Sr$ diagram (Fig. 9b) shows the new Merapi data from this study together with previously published data for other Javanese volcanoes that were used to define the Java field in Fig. 9a. As already indicated in Fig. 9a, the Merapi data extend to the high $^{87}Sr/^{86}Sr$ side of the field defined by volcanic rocks from elsewhere in Java and define a separate field displaced to somewhat higher $^{87}Sr/^{86}Sr$ at similar $^{143}Nd/^{144}Nd$ ratios compared with many Javanese volcanoes and the mantle array (Fig. 9b).

$^{206}Pb/^{204}Pb$ ratios for the studied Merapi rocks range from 18·73 to 18·78 (Table 1) and fall more or less within the range of published $^{206}Pb/^{204}Pb$ ratios (Whitford, 1975*a*; Del Marmol, 1989; McDermott & Hawkesworth, 1991; Turner & Foden, 2001). Slightly larger variations can be observed in $^{207}Pb/^{204}Pb$ ratios, which range from 15·68 to 15·72, and $^{208}Pb/^{204}Pb$ ratios, which vary from 39·02 to 39·22 (Table 1). Compared with the results from McDermott & Hawkesworth (1991), the Pb isotope ratios for Merapi from this study show a wider compositional range and generally more radiogenic values. In contrast to the Sr and Nd isotopic ratios there is no apparent systematic difference in Pb isotopic ratios between the two magmatic series.

Despite the small compositional differences, well-defined positive correlations can be observed in diagrams of $^{207}Pb/^{204}Pb$ and $^{208}Pb/^{204}Pb$ vs $^{206}Pb/^{204}Pb$ (Fig. 10). In terms of $^{206}Pb/^{204}Pb$ ratios, the Merapi data plot towards and beyond the radiogenic $^{206}Pb/^{204}Pb$ end of the Indian Ocean MORB array. $^{207}Pb/^{204}Pb$ and $^{208}Pb/^{204}Pb$ ratios for Merapi are significantly higher than typical Indian Ocean MORB values and within the range of volcanic rocks from Java and marine sediments from the Indian Ocean, which generally overlap the field of the Merapi volcanics in plots of $^{207}Pb/^{204}Pb$ and $^{208}Pb/^{204}Pb$ vs $^{206}Pb/^{204}Pb$. The Merapi rocks plot well above the Northern Hemisphere Reference Line (NHRL) and close to or within the field of OIB from the Indian Ocean in diagrams of $^{207}Pb/^{204}Pb$ vs $^{206}Pb/^{204}Pb$ and $^{208}Pb/^{204}Pb$ vs $^{206}Pb/^{204}Pb$, respectively.

Oxygen isotope data

Oxygen isotope data of Merapi are presented in Table 1. Whole-rock $\delta^{18}O$ values exhibit a range from +6·0 to +8·3‰. These values are slightly above typical values for MORB, which have uniform oxygen isotopic compositions with a total range in $\delta^{18}O$ values between +5·2 and +6·4‰ and average $\delta^{18}O$ values of +5·7 ± 0·2‰ (Harmon & Hoefs, 1995). The elevated $\delta^{18}O$ values of the Merapi volcanics relative to MORB may point to the assimilation of crustal material during magma ascent or storage in a shallow magma reservoir. However, secondary processes such as hydration and weathering can also cause substantial increases in $\delta^{18}O$ values of fine-grained, porous and glassy volcanic rocks (e.g. Taylor, 1968; Taylor & Turi, 1976; Ferrara *et al.*, 1985). Whole-rock data from Merapi show a marked positive correlation of $\delta^{18}O$ with LOI (Fig. 11). This finding is consistent with an increase in $\delta^{18}O$ by hydration and oxygen exchange between meteoric waters and the glassy groundmass of the pumiceous Merapi rocks, which are particularly susceptible to low-temperature alteration processes. Oxygen isotope analyses were made on plagioclase separates from some of the same rocks, as plagioclase is not as susceptible to secondary alteration as glass. The $\delta^{18}O$ values determined on plagioclase separates range from +6·5 to +7·0‰. The plagioclase phenocrysts have $\delta^{18}O$ values that are 0·2–1·3‰ lower than those of the corresponding whole-rock composition (Table 1). In unaltered rocks, where the groundmass is in equilibrium with the phenocrysts, the maximum difference between whole rock and plagioclase should be between 0·2 and 0·5‰, the whole rock having the higher values (Taylor & Turi, 1976). At Merapi, the difference between whole rock and plagioclase is about 0·2–0·3‰ in the unaltered samples and reaches a maximum of 1·3‰ in the most altered rocks (Table 1). This result is best explained by hydration of glass in pumiceous samples. Therefore, only oxygen isotope data from plagioclase separates and unaltered whole-rock samples can be used to make inferences about magma genesis at Merapi. Maximum magmatic $\delta^{18}O$ values of approximately +7·0‰ might be inferred from the linear relationship between $\delta^{18}O$ and LOI used to correct the effects of low-temperature alteration, as illustrated in Fig. 11, and the $\delta^{18}O$ values of plagioclase phenocryst separates. An important observation is that even without adjustment for secondary water take-up, both medium-K and high-K series volcanic rocks display a similar range in oxygen isotope ratios (Table 1).

DISCUSSION

The role of crustal contamination in the petrogenesis of the Merapi magmas

Many studies on arc magma genesis have provided clear evidence for the assimilation of crustal material as an important process of modification of the trace element and isotopic composition of mantle-derived arc magmas (Davidson, 1987; Hildreth & Moorbath,

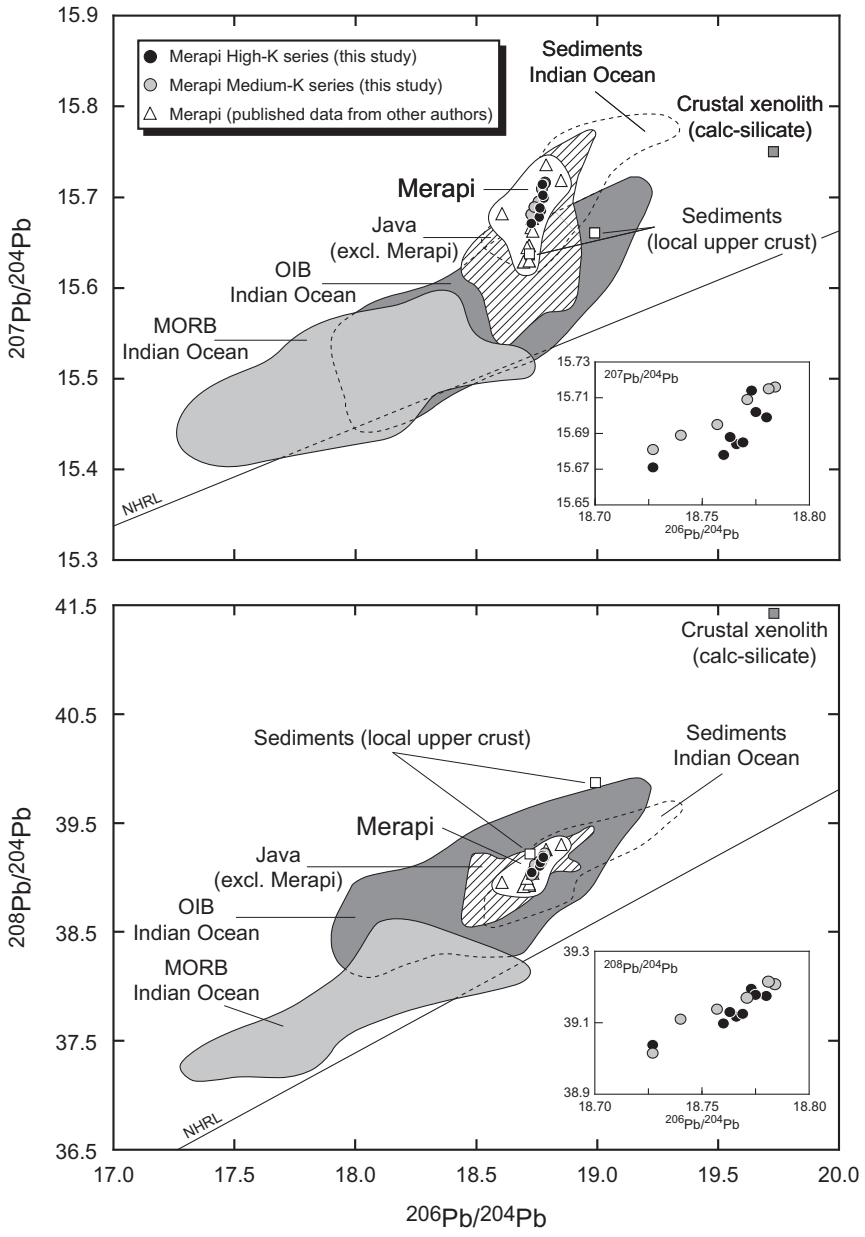

Fig. 10. $^{207}Pb/^{204}Pb$ and $^{208}Pb/^{204}Pb$ vs $^{206}Pb/^{204}Pb$ isotope diagrams showing data from Merapi compared with Indian Ocean MORB and OIB (St. Paul, Crozet, New Amsterdam, Mascarene Islands, Kerguelen, Heard Island), volcanic rocks from Java (excluding Merapi) and marine sediments from the Indian Ocean. Analyses of a crustal xenolith found in the Merapi lavas and sediments from the local upper crust (Table 2) are shown for comparison. NHRL (Northern Hemisphere Reference Line) from Hart (1984). Data sources: MORB, Indian Ocean (Dupré & Allègre, 1983; Hamelin & Allègre, 1985; Ito *et al*., 1987; Rehkämper & Hofmann, 1997); OIB, Indian Ocean (Dosso *et al*., 1979, 1988; Dupré & Allègre, 1983; Hamelin *et al*., 1985; Barling & Goldstein, 1990; Yang *et al*., 1998); Java (Whitford, 1975*a*; Edwards *et al*., 1991, 1993; Turner & Foden, 2001); marine sediments, Indian Ocean (Ben Othman *et al*., 1989; Gasparon & Varne, 1998); published data, Merapi (Whitford, 1975*a*; Del Marmol, 1989; McDermott & Hawkesworth, 1991; Turner & Foden, 2001).

1988; Davidson & Harmon, 1989; Davidson *et al*., 1990; Ellam & Harmon, 1990; Thirlwall *et al*., 1996). In a general evaluation of crustal contamination vs subducted sediment input in western Sunda arc volcanics, Gasparon & Varne (1998) strongly argued for contamination of the primary magmas by the arc crust as an important feature of Sunda arc magmatism. Therefore, before characterizing the source components of the Merapi volcanics, it is essential to evaluate the likelihood of crustal contamination

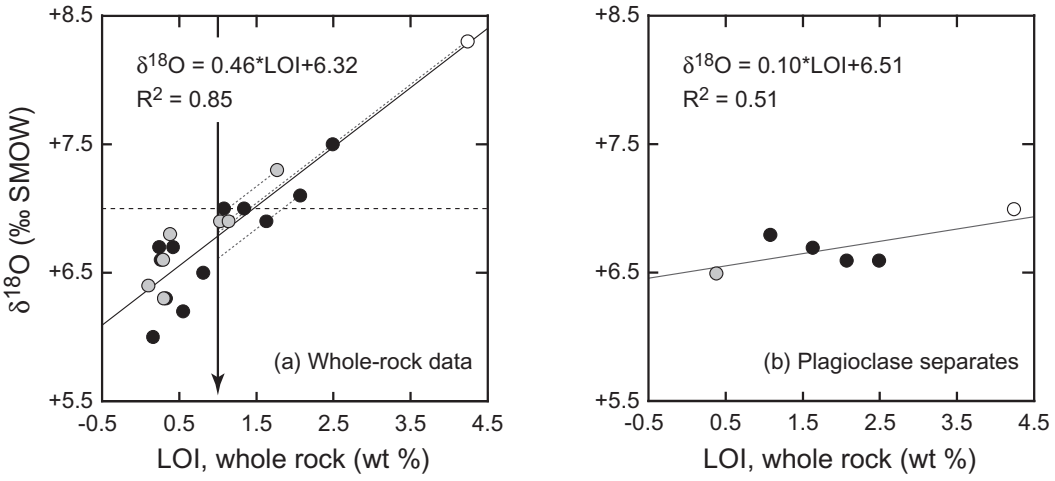

Fig. 11. $\delta^{18}O$ values (‰ SMOW) of Merapi whole rocks and plagioclase separates plotted against loss on ignition (LOI) (wt %), as determined on whole-rock samples. (a) Variation between $\delta^{18}O$ and LOI for the Merapi whole-rock data. The positive correlation indicates that a systematic enrichment in ^{18}O accompanies hydration during low-temperature alteration. For samples with LOI >1·0 wt %, a series of extrapolations down to an LOI value of 1·0 wt % have been made along lines parallel to a least-squares regression line (continuous line) through the dataset to correct for the effects of low-temperature alteration. The correction procedure suggests maximum magmatic $\delta^{18}O$ values of approximately +7·0‰ for Merapi, as indicated by the dashed horizontal line. (b) $\delta^{18}O$ values of plagioclase separates from some of the analysed whole-rock samples. The data indicate that plagioclase crystals are relatively unaffected by alteration processes, thus providing an independent estimate of the $\delta^{18}O$ values of the Merapi magmas. Symbols as in Fig. 3.

of mantle-derived magmas during ascent through the arc crust and possible effects on magma compositions at Merapi.

As in most volcanic arcs, what are considered primary magma compositions are comparatively rare in the Sunda arc (Whitford *et al*., 1979; Carn & Pyle, 2001) and apparently absent at Merapi (Del Marmol, 1989; Berthommier, 1990; Andreastuti, 1999; Gertisser, 2001). This indicates that even the most primitive Merapi rocks have been affected to some degree by evolutionary processes during magma ascent and may have assimilated crustal material en route to the surface. At first sight, the elevated LILE concentration in the high-K relative to the medium-K series rocks and the general correlation with $^{87}Sr/^{86}Sr$ isotope ratios appear consistent with a model involving contamination of mantle-derived magmas during ascent, with differentiation processes at shallower depths generating the observed compositional variations. In fact, the abundance of calcareous xenoliths within the Merapi volcanic rocks provides evidence for the interaction of magmas with crustal lithologies typical of the subvolcanic basement of the volcano. Nevertheless, the geochemical characteristics of the Merapi volcanics suggest that any compositional effects from interaction with the arc crust are negligible. The inferred magmatic $\delta^{18}O$ values estimated for Merapi ($\delta^{18}O \leq 7{\cdot}0$‰) still lie within the mantle range for oceanic basalts and only slightly above $\delta^{18}O$ values typical of MORB (Harmon & Hoefs, 1995), indicating that the extent of crustal contamination is limited. An important observation is that the high-K series rocks have fairly constant oxygen isotope ratios similar to those of the medium-K series rocks (Table 1; Fig. 12). This is strong evidence that the K-enriched character of the Merapi high-K series rocks is not related to contamination by ^{18}O-enriched crust at shallow crustal levels, as such a process would result in a sharp increase in oxygen isotope ratios concomitant with comparatively small $^{87}Sr/^{86}Sr$ variations within the series. As illustrated in Fig. 12, radiogenic and oxygen isotopic ratios within the individual magmatic series at Merapi are rather homogeneous. The high-K series rocks have nearly constant $^{87}Sr/^{86}Sr$ ratios that are distinctly higher than those of the medium-K series volcanics and generally lower $^{143}Nd/^{144}Nd$ ratios. Moreover, both magmatic series lack any systematic variation in $^{87}Sr/^{86}Sr$ and $^{143}Nd/^{144}Nd$ ratios with SiO_2. Lead and oxygen isotope ratios are scattered and independent of the geochemical affinity and the degree of differentiation of the samples. The combined radiogenic and oxygen isotopic data thus preclude a significant role for crustal contamination by combined assimilation–fractional crystallization (AFC) (DePaolo, 1981) or bulk crustal contamination in the petrogenesis and evolution of the magmas. As the isotopic ratios of the magmas appear to remain relatively unchanged during magmatic differentiation (Fig. 12), similar isotopic ratios might be inferred for the evolved and basic or parental magma compositions of each

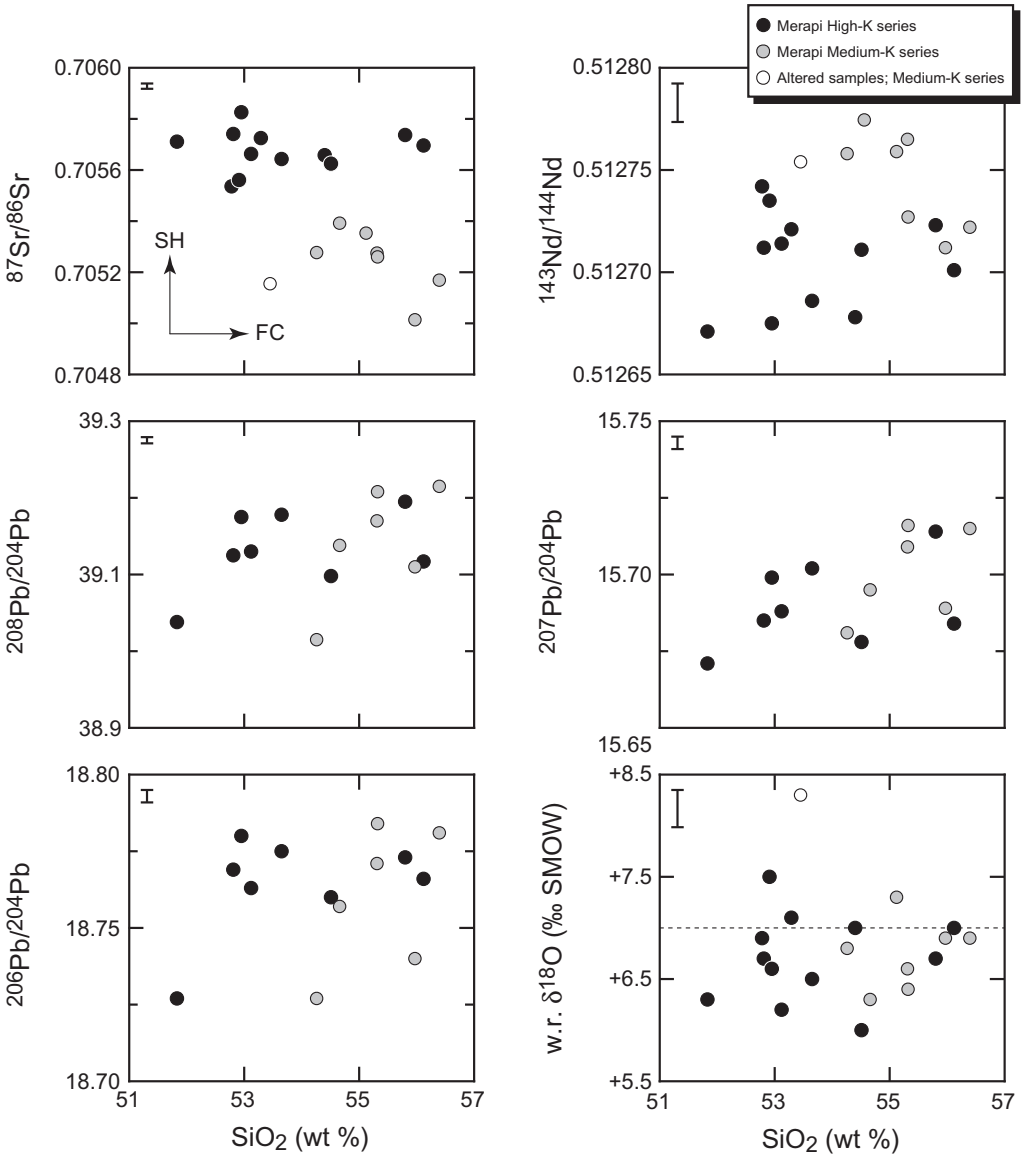

Fig. 12. Variation diagrams for Sr, Nd, Pb and O isotopic ratios vs SiO_2 (wt %) for Merapi medium-K and high-K series rocks. Arrows in the $^{87}Sr/^{86}Sr$ vs SiO_2 diagram labelled FC and SH indicate general differentiation trends within each series produced by fractional crystallization (FC) and variation in parental magmas related to source heterogeneity (SH). The dashed horizontal line marks the upper limit of primary magmatic $\delta^{18}O$ values for Merapi, as inferred from Fig. 11. Error bars (2σ) of the reported isotopic ratios are shown in the upper left corners. w.r., whole rock.

magmatic series, which may ultimately reflect the isotopic composition of the mantle source. Accordingly, models involving the derivation of the Merapi high-K magmas by crustal contamination of less K-rich primary magmas appear to be less likely. Instead, the rather low $\delta^{18}O$ values and the difference in radiogenic isotope composition between the Merapi volcanics and MORB-source mantle are interpreted to result to a great extent from the relative contributions of different components in the source region of the Merapi magmas.

Source characteristics of the Merapi magmas

Composition of the mantle wedge before the addition of slab-derived components

As discussed above, the Merapi magmas appear to be largely unaffected by crustal contamination. Accordingly, the geochemical characteristics of the most primitive volcanic rocks are interpreted to reflect their mantle source region, which must be heterogeneous. Introduction of slab-derived material may cause

substantial and heterogeneous changes in the radiogenic isotope composition of the mantle wedge and hence the isotopic signature of melts derived from it. However, the extent of these subduction-related changes on arc magmas critically depends on the inferred isotopic composition of the unmodified mantle wedge before subduction modification. This is illustrated by the $^{87}Sr/^{86}Sr$ and $^{143}Nd/^{144}Nd$ ratios of the Merapi volcanics that are displaced from the field of Indian Ocean MORB and show restricted overlap with the field defined by OIB from the Indian Ocean (Fig. 9a). Thus, in the case of an assumed unmodified MORB-like mantle source, the generation of the isotopic signatures of Merapi requires rather strong subduction-related changes in the mantle wedge. Alternatively, in the case of a more enriched mantle with higher $^{87}Sr/^{86}Sr$ and lower $^{143}Nd/^{144}Nd$ ratios than MORB, the addition of subduction-zone components, although still required to account for many of the isotopic and trace element characteristics of the Merapi volcanics, would have comparatively little effect on the isotopic composition of the mantle wedge.

In the case of the Sunda arc, MORB-like $^{3}He/^{4}He$ ratios of mantle xenoliths from Bukit Telor Volcano in Sumatra (Gasparon *et al*., 1994) and volcanoes between western Java and Flores (Hilton & Craig, 1989) suggest a MORB-like mantle as the dominant source of primary magmas along the entire length of the arc. This finding is corroborated by studies of tholeiitic and calc-alkaline volcanic rocks from Flores (Stolz *et al*., 1990) and Java (Gerbe *et al*., 1992; Edwards *et al*., 1993; Turner & Foden, 2001), which have $^{143}Nd/^{144}Nd$ ratios only slightly below those of Indian Ocean MORB and at the upper limit of typical Indian Ocean OIB values. In addition, there are indications for a contribution from an enriched mantle component (e.g. Stolz *et al*., 1990; Edwards *et al*., 1991, 1994; Van Bergen *et al*., 1992). Further constraints on the nature of the mantle wedge below Merapi may be placed by the concentrations of HREE and the HFSE in particular. In contrast to LILE and LREE, these elements are assumed to be fluid immobile and not enriched in the mantle wedge by processes related to slab dehydration (Pearce, 1983). Accordingly, the abundances and ratios of HFSE in the source of volcanic arc magmas should be insensitive to the introduction of components from the slab and may be used to examine the composition of the sub-arc mantle before metasomatism by slab-derived components (McCulloch & Gamble, 1991; Woodhead *et al*., 1993). Assuming that inter-element fractionation of highly incompatible trace elements is insignificant during relatively high-degree partial melting of peridotitic mantle, element ratios such as Zr/Nb in the magma should reflect the composition of the unmodified mantle wedge. At Merapi, Zr/Nb ratios are similar for the medium-K and high-K series eruptive products (Zr/Nb ~24·2–33·5 and ~26·2–32·2, respectively; Table 3) and vary within the range typical of MORB (Zr/Nb ~30; Sun & McDonough, 1989). The mantle source of the Merapi magmas may, therefore, be similar to an N-type MORB source. Furthermore, the Merapi volcanics are characterized by higher Ta/Nb ratios than MORB and OIB, which have chondritic Ta/Nb ratios (Jochum *et al*., 1986). Although comparison of Ta/Nb ratios measured for Merapi rocks with those of other subduction-related volcanics is restricted because of the lack of high-precision Ta and Nb data, the Ta/Nb ratios (with an average value of 0·07–0·08; Table 3) obtained for the Merapi medium-K and high-K series rocks largely overlap with those from other arc volcanoes (e.g. Feeley & Davidson, 1994; Elliott *et al*., 1997; Peate *et al*., 1997). Non-chondritic Ta/Nb ratios in arc volcanics may be taken as indicative of a more depleted MORB-like mantle source beneath many subduction zones (Woodhead *et al*., 1993), as Nb is thought to be slightly more incompatible than Ta during partial melting of peridotitic mantle (Green *et al*., 1989). Repeated episodes of melt extraction from the upper mantle will therefore create increasingly depleted residues with elevated Ta/Nb ratios. Accordingly, incompatible trace element ratios in the Merapi volcanics may be used to infer a MORB-like mantle wedge or possibly the depleted residue of MORB-source mantle following a previous episode of melt extraction.

The ratios of immobile trace elements such as Ta/Nb, Zr/Nb and Zr/Hf are similar for most Merapi volcanics (Table 3) and not systematically related to temporal relations or stratigraphy. The similarity of these trace element ratios in the medium-K and high-K series eruptives provides good evidence for a homogeneous mantle source with affinity to that of the source of N-MORB before subduction-related compositional change in the mantle wedge. Previous melt depletion of the sub-arc mantle makes it highly susceptible to the addition of material rich in incompatible trace elements from the subducted plate, which is considered a controlling factor in determining the overall compositional variation in the abundances and ratios of incompatible trace elements between the medium-K and high-K series rocks of Merapi.

Identification of slab-derived components in the genesis of the Merapi magmas

Constraints from isotope data. Given that the mantle wedge beneath Merapi appears to have characteristics of an N-type MORB source, the co-variation of Sr and

Table 3: Average trace element ratios for N-MORB (Sun & McDonough, 1989) and Indian Ocean sediments (see Fig. 13) (Gasparon & Varne, 1998; Plank & Langmuir, 1998) and the average and range for the Merapi medium-K and high-K series rocks

	N-MORB	Indian Ocean sediments			Merapi	
		Sed.-A	Sed.-B	Sed.-C	Medium-K series	High-K series
Zr/Nb	31·8	13·2	11·9	20·1	27·8 (24·2–33·5)	28·8 (26·2–32·2)
Ta/Nb	0·06	0·08	0·06	0·09	0·08 (0·07–0·09)	0·07 (0·07–0·08)
Zr/Hf	36·1	30·6	35·8	36·1	42·1 (39·7–43·9)	40·1 (36·4–43·5)
B/Nb	—	—	—	—	3·5 (2·6–4·1)	5·7 (4·2–7·3)
Ba/Nb	2·7	97·8	6·8	20·8	122·4 (93–172)	162·2 (129–192)
Th/Nb	0·05	0·9	0·4	1·2	1·6 (1·2–2·4)	2·3 (2·0–2·7)
Ce/Nb	3·2	7·9	3·0	4·8	9·1 (8·2–11·1)	11·6 (9·6–13·1)
B/Zr	—	—	—	—	0·13 (0·11–0·15)	0·20 (0·16–0·24)
Ba/Zr	0·09	7·38	0·81	1·03	4·37 (3·82–5·12)	5·61 (4·88–6·36)
Th/Zr	0·002	0·068	0·042	0·058	0·057 (0·044–0·071)	0·080 (0·073–0·090)
Ce/Zr	0·10	0·60	0·36	0·24	0·33 (0·29–0·37)	0·40 (0·36–0·42)
Ce/Pb	25·0	3·4	3·9	2·2	2·1 (1·7–2·7)	2·1 (1·4–2·9)
B/Be	—	—	—	—	14·4 (9·6–18·2)	18·1 (15·0–21·5)
Ba/La	2·5	27·3	5·9	9·3	27·4 (22·6–31·6)	27·7 (24·9–33·0)
Th/U	2·6	6·6	8·1	3·7	4·5 (3·8–5·1)	5·2 (4·5–6·0)

Nd isotope ratios defining a linear trend parallel to the mantle array and the displacement of Merapi Sr and Nd isotopic data away from the Indian Ocean MORB field (Fig. 9a) suggest the involvement of either a sedimentary or a crustal component in the genesis of the Merapi magmas. As discussed above, the Merapi magmas appear to be significantly unaffected by shallow crustal contamination. Therefore, the shift in Sr and Nd isotope ratios must be due to the addition of crustal material to the upper mantle from the descending slab. Variations in the Sr and Nd isotope compositions of the Merapi volcanics may be attributed to two-component mixing between a MORB-like mantle source and marine sediments from the Indian Ocean. Trace element characteristics of the Merapi volcanics, such as low Ce/Pb and high Th/Nb ratios (Ce/Pb $\sim$ 1·4–2·9, Th/Nb $\sim$ 1·2–2·7; Table 3) relative to MORB (Ce/Pb $\sim$ 25, Th/Nb $\sim$ 0·05; Table 3), provide good evidence for the introduction of sedimentary material into the mantle source of the magmas. This is corroborated by the $^{207}Pb/^{204}Pb$ and $^{208}Pb/^{204}Pb$ ratios of the Merapi rocks that are significantly higher than Indian Ocean MORB values and lie within the range of Indian Ocean marine sediments (Fig. 10). Mixing of two isotopically distinct components in plots of $^{207}Pb/^{204}Pb$ and $^{208}Pb/^{204}Pb$ vs $^{206}Pb/^{204}Pb$ ratios will yield linear arrays that project through the compositions of the end-member components involved. Hence, the linear trends defined by the Pb isotope data support our model involving mixing between a MORB-like mantle source and subducted Indian Ocean sediments. It is emphasized, however, that such a model requires a comparatively radiogenic Indian Ocean MORB composition and a rather specific sediment composition to be involved in the mixing process. This contamination of a MORB-like mantle and sediments from the slab is also considered to be the dominant process affecting the geochemical composition of the mantle source of other Quaternary volcanoes from Java (Figs 9, 10, 13 and 14) and the Sunda arc in general (Turner & Foden, 2001).

The model has, however, been questioned by Gasparon & Varne (1998), who concluded that assimilation of crustal material by ascending melts better accounts for the range and spatial distribution of the Sr, Nd and Pb isotope systematics of western Sunda arc volcanics than source contamination by subducted sediments. Support for their conclusion may be derived from the low ^{10}Be abundances in the Sunda arc volcanics (Tera *et al.*, 1986; Edwards *et al.*, 1993) and concomitant along-arc variations in crustal composition and thickness and isotope compositions of mafic arc volcanics. Although crustal assimilation cannot be excluded for some Sunda arc volcanoes, it is apparently

insignificant for Merapi, where the compositional effects of subducted sediment input prevail. Geophysical data suggest that the bulk of the marine sediments accumulating off the coast of Java are added to the accretionary wedge (Hamilton, 1979). A fraction of the sediment approaching Java is transported into and subducted along the Java trench and eventually carried into the mantle wedge (Hamilton, 1979; Plank & Langmuir, 1998). Even the overall low ^{10}Be concentrations of the Sunda arc volcanics do not preclude recycling of subducted sediments in the source region of the Merapi magmas. Taking into account modern subduction-zone geometry models and a subduction rate of 6–7 cm/yr (Hamilton, 1979; Jarrard, 1986; Widiyantoro & Van der Hilst, 1996, 1997), it will take ~6 Myr for subducted sediment to reach a depth of 190 km beneath Merapi. ^{10}Be would then be difficult to detect in the arc volcanics because of its half-life of 1·5 Ma (Yiou & Raisbeck, 1972).

In Fig. 13, $^{87}Sr/^{86}Sr$, $^{143}Nd/^{144}Nd$ and $^{206}Pb/^{204}Pb$ ratios are chosen to illustrate the effects on these isotopic systems of adding various amounts of Indian Ocean sediments to an Indian Ocean MORB source. As already illustrated in the $^{143}Nd/^{144}Nd$ vs $^{87}Sr/^{86}Sr$ diagram (Fig. 9a) the Merapi volcanics and those from elsewhere in Java do not overlap with the MORB field. Instead, $^{87}Sr/^{86}Sr$, $^{143}Nd/^{144}Nd$ and $^{206}Pb/^{204}Pb$ ratios for Merapi and other Javanese volcanoes are shifted away from the MORB field towards the Indian Ocean sediment field. Interestingly, the high-K series rocks are displaced further away from MORB towards the sediment field. There is limited overlap between the field defined by the Merapi rocks and that of Indian Ocean OIB, but some of the Merapi and Java data extend to values outside of this field, plotting between the fields for OIB and sediments. Two-component mixing arrays (Fig. 13) between an average Indian Ocean MORB and several Indian Ocean sediment compositions, which include (1) a composition representative of the sedimentary component approaching and entering the Java trench (Plank & Langmuir, 1998), (2) an Upper Cretaceous ooze from DSDP Site 211 (Gasparon & Varne, 1998) and (3) the average of terrigenous–biogenic sediments V33-75, -77 and -79 (Ben Othman *et al*., 1989; Gasparon & Varne, 1998), suggest that, as a first approximation, all Java volcanics can be fitted with bulk-mixing curves between a MORB-source mantle and typical Indian Ocean sediments. The same applies to the Merapi medium-K and high-K series rocks that also plot along possible bulk mixing arrays. The low Pb abundances in the MORB source relative to those in the sediment component require the addition of only a few percent of sediment to significantly alter the Pb isotope composition of the unmodified mantle source. In general, the calculations show that the addition of ~1–2% sediment to MORB-source mantle may be sufficient to generate the $^{87}Sr/^{86}Sr$, $^{143}Nd/^{144}Nd$ and $^{206}Pb/^{204}Pb$ ratios of the Merapi magmas. In extreme cases, and using the average of terrigenous–biogenic sediments V33-75, -77 and -79 (Sed.-C, Fig. 13), up to 10% sediment is required, although these sediments could be compositionally and isotopically different from those being subducted along the Java trench, as they were sampled in the vicinity of Java (Fig. 1) and might be largely derived from the arc itself (Gasparon & Varne, 1998). To account for the Sr, Nd and Pb isotopic signatures of the Merapi high-K series volcanics a slightly higher percentage of sediment is required in the mixture (Fig. 13). This result is consistent with the higher $^{87}Sr/^{86}Sr$ and generally lower $^{143}Nd/^{144}Nd$ ratios of the high-K series rocks relative to those of the medium-K series (Fig. 9), which may also be attributable to a slightly higher sediment component in the source of the high-K magmas.

Although the radiogenic isotope systematics of the Merapi volcanics are consistent with a process of source contamination by subducted sedimentary material, they cannot alone unequivocally exclude the assimilation of crustal material by the ascending magmas. The overall low oxygen isotope ratios of the Merapi volcanics provide more conclusive evidence that the contaminant—characterized by high Sr and Pb isotope ratios and low Nd isotope ratios—is essentially derived from subducted sediment added to the mantle source before the generation of the Merapi magmas. It is emphasized that this interpretation does not argue against contamination of uprising magmas, as indicated by the occurrence of calcareous xenoliths in the Merapi lavas, but that any possible compositional effect of contamination from the arc crust on the Merapi magmas is limited and merely superimposed on the effect of sediment subduction. As shown in Fig. 13, even small amounts of sediment mixed into peridotitic mantle may cause substantial changes in its radiogenic isotopic composition, whereas such a process will have little effect on oxygen isotope systematics. The effects of contamination of the mantle source on magmatic compositions may be visualized by considering the mixing relationships with respect to Sr and O isotope ratios (Fig. 14). Because of higher Sr concentrations in the crustal component than in the mantle source, mixing curves will be strongly convex downward, reflecting large changes in $^{87}Sr/^{86}Sr$ ratios at nearly constant $\delta^{18}O$ values produced by relatively small amounts of contamination. In contrast, crustal contamination of ascending magmas with initial Sr concentrations higher than those in the assimilated crustal material will more markedly affect O isotopes rather than Sr isotope ratios (James, 1981). The

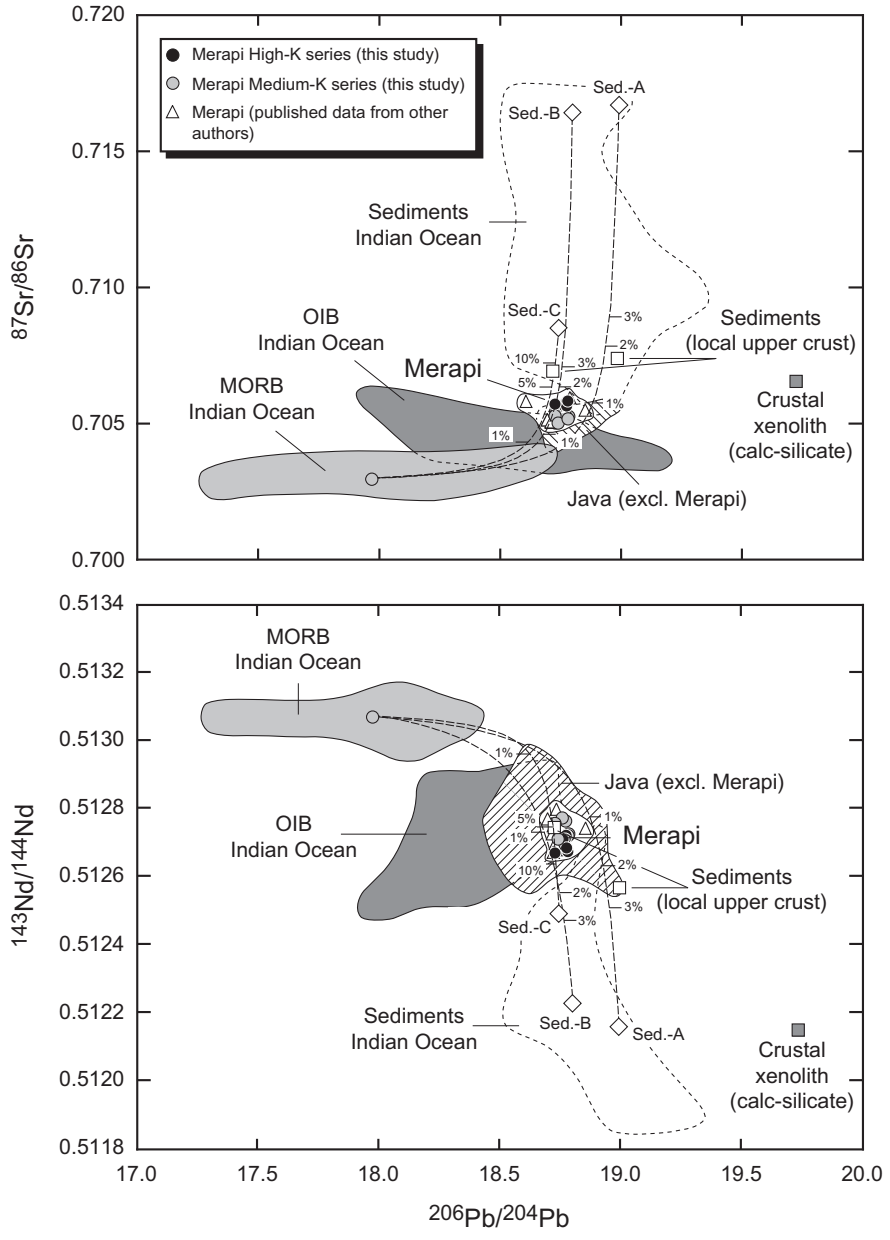

Fig. 13. $^{87}Sr/^{86}Sr$ and $^{143}Nd/^{144}Nd$ vs $^{206}Pb/^{204}Pb$ isotope diagram showing data from Merapi relative to Indian Ocean MORB and OIB, volcanic rocks from Java (excluding Merapi), marine sediments from the Indian Ocean, a crustal xenolith and sediments from the local upper crust (Table 2). Also illustrated are mixing arrays calculated between Indian Ocean MORB mantle and marine sediments. The ticks along the mixing curves indicate the percent of sediment in the mixture. Data sources: see Figs 9 and 10. End-member compositions used in the calculations: MORB mantle: Sr 9 ppm, Nd 0·73 ppm, Pb 0·03 ppm [0·1 × N-MORB values from Sun & McDonough (1989)], $^{87}Sr/^{86}Sr$ = 0·702991, $^{143}Nd/^{144}Nd$ = 0·513075, $^{206}Pb/^{204}Pb$ = 17·966; Sed.-A (average sediment, Java): Sr 218 ppm, Nd 34 ppm, Pb 25 ppm, $^{87}Sr/^{86}Sr$ = 0·716820, $^{143}Nd/^{144}Nd$ = 0·512160, $^{206}Pb/^{204}Pb$ = 18·990 (Plank & Langmuir, 1998); Sed.-B (nanno ooze, DSDP Site 211): Sr 126 ppm, Nd 52 ppm, Pb 18 ppm, $^{87}Sr/^{86}Sr$ = 0·71643, $^{143}Nd/^{144}Nd$ = 0·512228, $^{206}Pb/^{204}Pb$ = 18·772 (Gasparon & Varne, 1989); Sed.-C (terrigenous–biogenic, average value of V33-75, -77, -79): Sr 260 ppm, Nd 15 ppm, Pb 14 ppm, $^{87}Sr/^{86}Sr$ = 0·708513, $^{143}Nd/^{144}Nd$ = 0·512493, $^{206}Pb/^{204}Pb$ = 18·742 (Ben Othman *et al.*, 1989; Gasparon & Varne, 1998).

inferred magmatic $\delta^{18}O$ values of the Merapi volcanics within the upper range of typical mantle values and the displacement of the radiogenic isotope ratios from the MORB field are therefore consistent with admixing of continent-derived sediments into the mantle source. The Merapi medium-K and high-K series rocks all plot in a narrow range on the $\delta^{18}O$ vs $^{87}Sr/^{86}Sr$ diagram (Fig. 14), shifted from the MORB and the Java

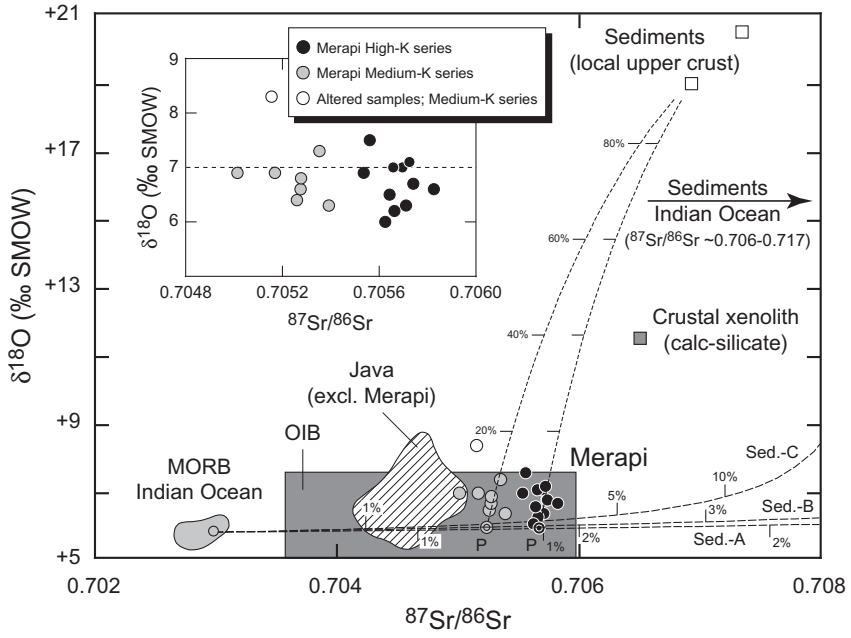

Fig. 14. $\delta^{18}O$ vs $^{87}Sr/^{86}Sr$ isotope diagram showing whole-rock data from Merapi relative to Indian Ocean MORB and OIB, volcanic rocks from Java (excluding Merapi), crustal rocks from Java (Table 2) and marine sediments from the Indian Ocean. The low $\delta^{18}O$ value of the calc-silicate xenolith compared with the local calcareous sediments suggests that the original $^{18}O/^{16}O$ ratio has been lowered by interaction with the Merapi magmas. Subduction-zone enrichment is shown by mixing curves between Indian Ocean MORB mantle and typical Indian Ocean sediments. Possible contamination by shallow crustal material is illustrated by theoretical bulk mixing curves between primary, mantle-derived magmas (P) and local sediments. The ratio of Sr concentration in the mantle-derived magmas to Sr concentration in the assimilated crustal rocks is assumed to be 2:1. Percentages of sediment or crust added are indicated along the curves. The dashed horizontal line in the inset marks the upper limit of primary magmatic $\delta^{18}O$ values of Merapi, as inferred from Fig. 11. Data sources: MORB, Indian Ocean (Ito *et al.*, 1987); OIB: $^{87}Sr/^{86}Sr$ variation as in Fig. 9, $\delta^{18}O$ range (Harmon & Hoefs, 1995). The Java field includes data from Galunggung (Gerbe *et al.*, 1992), Muriah (Edwards *et al.*, 1991) and Ringgit–Beser (Edwards *et al.*, 1994). Strontium isotopic compositions and concentrations for MORB and sediment end-members used in the calculations are the same as in Fig. 13. Oxygen isotope ratios: MORB mantle, $\delta^{18}O = +5{\cdot}75‰$ (SMOW); Sed.-A, -B, -C, $\delta^{18}O$ (assumed value) $= +16‰$ (SMOW).

field to higher $^{87}Sr/^{86}Sr$ ratios. Mixing calculations between Indian Ocean MORB mantle and Indian Ocean sediments (Fig. 14) yield results that are in general agreement with those obtained based on the interpretation of the $^{87}Sr/^{86}Sr$, $^{143}Nd/^{144}Nd$ and $^{206}Pb/^{204}Pb$ data (Fig. 13). Although the exact mixing ratio varies as a function of the sediment composition used in the model, the calculations suggest that (1) a small percentage of sediment may be sufficient to increase the $^{87}Sr/^{86}Sr$ ratios of the mantle wedge to values typical of the Merapi volcanics and (2) a slightly higher proportion of subducted sediment may be necessary to account for the average $^{87}Sr/^{86}Sr$ ratio of the high-K series rocks.

It may be noteworthy that the $^{87}Sr/^{86}Sr$ ratios of subduction-related magmas can also be shifted to somewhat higher values than MORB mantle as a result of the modification of the mantle wedge by fluids released from hydrothermally altered oceanic crust. In a way, this may reduce the amount of sediment addition required to explain the overall variation in $^{87}Sr/^{86}Sr$ ratios. However, as such a process does not affect Nd, it is not able to account for the observed variation in Nd isotope ratios. The mixing calculations (Fig. 14) also illustrate that the magmatic $\delta^{18}O$ values of Merapi are slightly higher than the predicted values for the MORB–sediment mixture. Although this may critically depend on the precise sediment composition used in the mixing model and the mode of transfer of the sedimentary material into the mantle wedge, the small increase in $\delta^{18}O$ values could, in fact, reflect small degrees of crustal contamination affecting the oxygen isotope composition of ascending magmas at Merapi. Although certainly an oversimplification of the actual contamination process, bulk mixing may be used to place an upper limit on the extent of contamination by shallow crustal material, as the isotopic and geochemical data are difficult to reconcile with simple AFC models. As depicted in Fig. 14, mixing models between primary, mantle-derived magmas and crustal material compositionally similar to the calcareous sediments of the local upper crust indicate that the theoretically maximum bulk crustal contamination of the Merapi magmas during ascent or storage in a shallow reservoir may be something in the order of a few percent, realistically less.

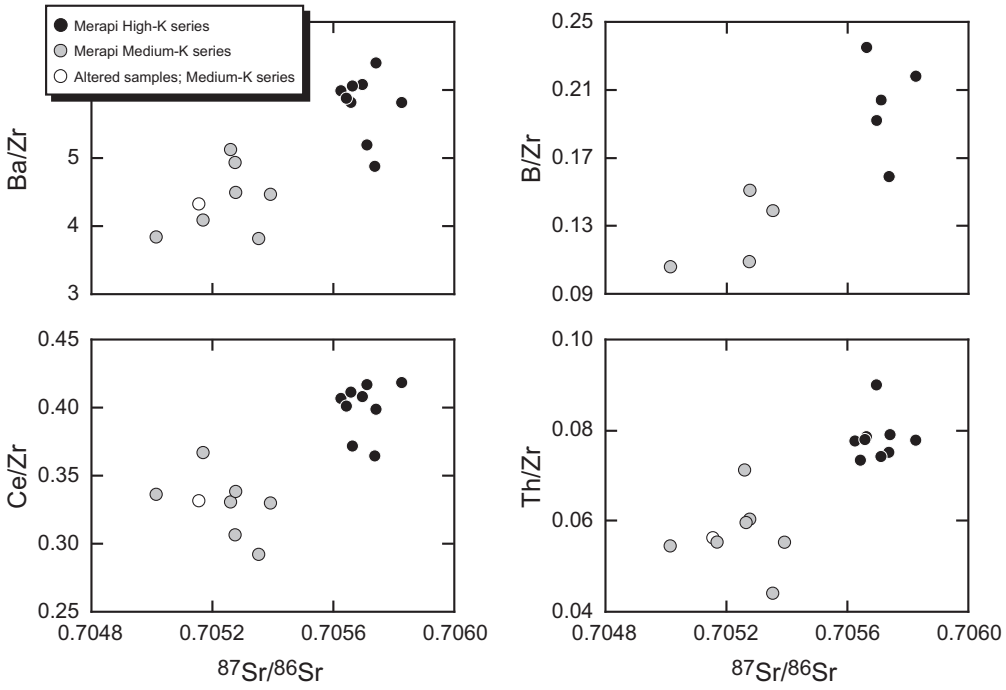

Fig. 15. Plots of Ba/Zr, B/Zr, Ce/Zr and Th/Zr vs $^{87}Sr/^{86}Sr$ for Merapi medium-K and high-K series rocks.

Constraints from trace elements. In the previous section it was shown that bulk-mixing models between sediment and unmodified MORB-source mantle are capable of explaining the variation of radiogenic and oxygen isotopic ratios in the Merapi volcanics. Moreover, it was proposed that derivation of the parental magmas of the medium-K and high-K series from isotopically distinct mantle sources, variably enriched by the addition of a sediment component from the subducted slab, can account for the systematic isotopic differences between them. However, although models involving bulk addition of subducted sediment to the mantle wedge are consistent with the observed variation of radiogenic and oxygen isotopes, they fail adequately to explain some of the incompatible trace element characteristics of the Merapi volcanics. Closer observation of the trace element data requires certain incompatible trace elements to be fractionated during transport of slab-derived components into the mantle wedge, suggesting that both aqueous metasomatism by slab fluids and hybridization by partial melts are important processes enriching the mantle source of the Merapi magmas rather than simple bulk addition of subducted sediment. For example, the typically spiked incompatible trace element patterns of the Merapi volcanics in a MORB-normalized multi-element diagram (Fig. 6) are highly distinctive features of arc lavas. These are commonly interpreted as evidence for the involvement of a fluid or melt contribution from the subducted slab. The resulting elevated LILE/HFSE, LREE/HFSE and Th/HFSE ratios of the Merapi rocks that are higher than typical MORB and, in many cases, exceed those of bulk Indian Ocean sediments (Table 3) suggest that bulk addition of subducted sediment to the mantle wedge or any two-component mixing array between bulk sediment and unmodified depleted mantle is unable to reproduce the observed trend in the Merapi volcanics.

The geochemical differences between the medium-K and high-K series rocks appear to reflect a mantle source region that has been influenced by the addition of variable amounts of a slab-derived component. The most enriched Merapi rocks (Merapi high-K series) display the highest abundances in fluid-mobile elements (B, K, Rb, Sr, Ba, Pb, U), LREE and Th (Fig. 8) and the most elevated LILE (and B)/HFSE, LREE/HFSE and Th/HFSE ratios (Table 3; Fig. 15). The concomitant enrichment of fluid-mobile elements and elements, such as LREE and Th, that are thought to be much less readily transported by an aqueous fluid phase, suggests that both aqueous fluids and silicate melts were involved in transferring material from the slab to the mantle wedge.

The HREE concentrations of 10–15 times chondritic values (Fig. 7) and the isotopic evidence for the involvement of subducted sediment argue against a significant role of residual garnet in the petrogenesis of the Merapi magmas and suggest that the subducted

sediment component was added as a partial melt carrying Th and LREE into the source region of the Merapi magmas. However, it is clear that, to be able to reproduce the elevated Th/HFSE and LREE/HFSE of the Merapi volcanics relative to some of the bulk sediment compositions (Table 3) by mixing of a subducted sediment component with MORB-source mantle, the added sediment-derived partial melt is required to have higher Th/HFSE and LREE/HFSE ratios than the bulk sediment and to fractionate significantly LREE and Th from other HFSE, such as Zr and Nb, which have to be largely retained in the sediment residue (Elliot *et al.*, 1997).

Because of the relative mobility of LILE in aqueous fluids compared with HFSE, the enrichment of the former in subduction-related volcanic rocks relative to MORB is commonly linked to the flux of water derived from dehydration reactions in the subducting slab (Tatsumi *et al.*, 1986; Brenan *et al.*, 1995*a*, 1995*b*, 1998; Liu *et al.*, 1996; You *et al.*, 1996; Kogiso *et al.*, 1997; Tatsumi & Kogiso, 1997; Ayers, 1998). Accordingly, LILE/HFSE ratios should be highly sensitive to the addition of a slab-derived fluid phase to the mantle source. The elevated LILE concentrations and LILE/HFSE ratios (e.g. Ba/Zr) in the high-K relative to the medium-K series rocks (Table 3; Fig. 15) are therefore taken as indicative of a higher fluid component—identified by high LILE/HFSE ratios—in the mantle source of the high-K series magmas. The positive Ba/Zr vs $^{87}Sr/^{86}Sr$ trend (Fig. 15) suggests that the fluid component lies at higher $^{87}Sr/^{86}Sr$ values (and lower $^{143}Nd/^{144}Nd$ ratios) than the Merapi volcanics. Subducted sediment is, therefore, considered a major source of fluid-mobile elements in the source region of the Merapi magmas. It is worth stressing that this does not necessarily argue against a contribution of hydrous fluids from altered oceanic crust as inferred for many Sunda arc lavas (Turner & Foden, 2001). However, our data suggest that the subducted sediment component dominates both the flux of hydrous fluids and the addition of partial melts to the sub-arc mantle source of the Merapi magmas, largely controlling the overall isotopic and geochemical variation observed at Merapi. The degree of partial melting in the mantle wedge, which may be directly related to the fluid flux from the slab, might be another factor determining the concentrations of incompatible trace elements in the primary magmas of the different magmatic series. A slightly higher degree of partial melting induced by a higher flux of water from the slab may account for the lower abundances of immobile trace elements in the high-K relative to the medium-K series rocks (Fig. 8). Trace element ratios that are assumed to be largely unaffected by the subduction process (e.g. Ta/Nb, Zr/Nb, Zr/Hf) suggest that the mantle wedge beneath Merapi was relatively homogeneous in composition before any modification related to subduction processes, providing further evidence for variable mantle source enrichment beneath Merapi.

SUMMARY AND CONCLUSIONS

Lavas and pyroclastic rocks erupted from Merapi over the past few thousand years and possibly back to pre-Holocene time show a restricted range in SiO_2 (48·3–57·3 wt %) but vary significantly in their K_2O contents, allowing a medium-K and a high-K series to be distinguished. Both magmatic series show enrichment in LILE and LREE relative to HFSE, and elevated LILE/HFSE and LREE/HFSE ratios compared with MORB. The negative correlation between $^{87}Sr/^{86}Sr$ and $^{143}Nd/^{144}Nd$ and the displacement of the Merapi data away from the MORB field towards more radiogenic Sr isotopic compositions are suggestive of a contribution from a crustal component to the genesis of the Merapi magmas. Consistent with this conclusion are Pb isotope compositions that lie outside the range of MORB and within the field defined by Indian Ocean marine sediments. Oxygen isotope ratios for whole-rock samples from Merapi range from +6·0 to +8·3‰ relative to SMOW. Trends towards elevated $\delta^{18}O$ values are interpreted to reflect post-eruptive hydration and exchange of oxygen between ground water and volcanic glass. Plagioclase $\delta^{18}O$ values are generally lower ($\delta^{18}O \leq 7{\cdot}0$‰) than those measured for whole-rock samples. The low $\delta^{18}O$ values of the Merapi magmas limit the amount of high-level crustal contamination and provide evidence for contributions from subducted continental material to the source region of the Merapi magmas. This interpretation is corroborated by the lack of systematic variation between isotopic ratios and SiO_2, which suggest that crustal contamination by assimilation processes or bulk crustal contamination has not contributed significantly to the isotopic composition of the Merapi suite. In this respect, Merapi is similar to other Javanese volcanoes, such as Galunggung (Gerbe *et al.*, 1992), Guntur (Edwards *et al.*, 1993) and Ringgit–Beser (Edwards *et al.*, 1994), where low $\delta^{18}O$ values suggest that contamination by the arc crust is of minor importance compared with mantle source enrichment by a subducted sediment component.

Contrasts between the geochemical and radiogenic isotope compositions of eruptives from the medium-K and high-K series of Merapi and the similarity of oxygen isotope ratios within both suites can be reconciled with a model of variable source enrichment by subducted sedimentary material. Isotopic mixing calculations between MORB-source mantle and typical

Indian Ocean sediments suggest that, in general, addition of a few percent (~1–10%) sediment into the mantle wedge is sufficient to explain the radiogenic isotope compositions of the Merapi volcanics. A slightly larger contribution from sediment-derived aqueous fluids and partial melts to the source of the high-K series magmas can account for the trace element and isotopic contrasts between the two series.

The stratigraphy and chronology of the Middle to Late Holocene pyroclastic successions of Merapi provide clear evidence for an abrupt shift in the K_2O content of the eruptive products with time. Lavas from the somma rim and HPS deposits older than ~1900 ^{14}C years BP belong to the medium-K series, whereas all younger eruptive products have high-K composition (Gertisser, 2001; Gertisser & Keller, 2003). The transition from medium-K to high-K magmas is not believed to be directly related to processes occurring within the volcanic system nor to the structural evolution of the shallow volcanic complex, as might be inferred from the apparent coincidence with a possible major structural modification caused by a collapse of the western flank of the volcanic edifice (Newhall *et al*., 2000). The temporal change in the K_2O content is instead interpreted to be source-related rather than a reflection of shallow (intracrustal) processes and is a response to variations in the mantle wedge, with the primary high-K magmas being derived from a mantle source more markedly enriched by a subducted sediment component.

ACKNOWLEDGEMENTS

This study is part of German–Indonesian collaborative research at Merapi, co-ordinated by Jochen Zschau (GeoForschungsZentrum Potsdam). We are grateful to the directors and scientific staff of the Volcanological Survey of Indonesia in Bandung and the Volcano Technology Research Center (BPPTK) in Yogyakarta for hospitality and invaluable support in the field. Muharrem Satir (Universität Tübingen) kindly provided the isotope analyses. Comments and suggestions provided by Paul Hoskin were of considerable value. We thank John Gamble, David Pyle and Simon Turner for constructive reviews, and Marjorie Wilson for her careful review and editorial handling. This study was funded by the Deutsche Forschungsgemeinschaft through grant KE 136/31 to J.K.

REFERENCES

Andreastuti, S. D. (1999). Stratigraphy and geochemistry of Merapi Volcano, Central Java, Indonesia: implication for assessment of volcanic hazards. Ph.D. thesis, University of Auckland, New Zealand.

Andreastuti, S. D., Alloway, B. V. & Smith, I. E. M. (2000). A detailed tephrostratigraphic framework at Merapi Volcano, Central Java, Indonesia: implications for eruption predictions and hazard assessment. *Journal of Volcanology and Geothermal Research* **100**, 51–67.

Arculus, R. J. & Powell, R. (1986). Source component mixing in the regions of arc magma generation. *Journal of Geophysical Research* **91**, 5913–5926.

Ayers, J. (1998). Trace element modeling of aqueous fluid–peridotite interaction in the mantle wedge of subduction zones. *Contributions to Mineralogy and Petrology* **132**, 390–404.

Barling, J. & Goldstein, S. L. (1990). Extreme isotopic variations in Heard Island lavas and the nature of mantle reservoirs. *Nature* **348**, 59–62.

Ben Othman, D., White, W. M. & Patchett, J. (1989). The geochemistry of marine sediments, island arc magma genesis and crust–mantle recycling. *Earth and Planetary Science Letters* **94**, 1–21.

Berthommier, P. C. (1990). Étude volcanologique du Merapi (Centre-Java). Téphrostratigraphie et chronologie—produits éruptifs. Ph.D. thesis, Université Blaise Pascal, Clermont-Ferrand.

Brenan, J. M., Shaw, H. F. & Ryerson, F. J. (1995*a*). Experimental evidence for the origin of lead enrichment in convergent-margin magmas. *Nature* **378**, 54–56.

Brenan, J. M., Shaw, H. F., Ryerson, F. J. & Phinney, D. L. (1995*b*). Mineral–aqueous fluid partitioning of trace elements at 900 °C and 2·0 GPa: constraints on the trace element chemistry of mantle and deep crustal fluids. *Geochimica et Cosmochimica Acta* **59**, 3331–3350.

Brenan, J. M., Shaw, H. F. & Ryerson, F. J. (1998). The role of aqueous fluids in the slab-to-mantle transfer of boron, beryllium, and lithium during subduction: experiments and models. *Geochimica et Cosmochimica Acta* **62**, 3337–3347.

Camus, G., Gourgaud, A., Mossand-Berthommier, P.-C. & Vincent, P. M. (2000). Merapi (Central Java, Indonesia): an outline of the structural and magmatological evolution, with a special emphasis to the major pyroclastic events. *Journal of Volcanology and Geothermal Research* **100**, 139–163.

Carn, S. A. & Pyle, D. M. (2001). Petrology and geochemistry of the Lamongan Volcanic Field, East Java, Indonesia: primitive Sunda arc magmas in an extensional tectonic setting? *Journal of Petrology* **42**, 1643–1683.

Curray, J. R., Shor, G. G., Raitt, R. W. & Henry, M. (1977). Seismic refraction and reflection studies of crustal structure of the eastern Sunda and western Banda arcs. *Journal of Geophysical Research* **82**, 2479–2489.

Davidson, J. P. (1987). Crustal contamination vs subduction zone enrichment: examples from the Lesser Antilles and implications for mantle source compositions of island arc volcanic rocks. *Geochimica et Cosmochimica Acta* **51**, 2185–2198.

Davidson, J. P. & Harmon, R. S. (1989). Oxygen isotope constraints on the petrogenesis of volcanic arc magmas from Martinique, Lesser Antilles. *Earth and Planetary Science Letters* **95**, 255–270.

Davidson, J. P., McMillan, N. J., Moorbath, S., Wörner, G., Harmon, R. S. & Lopez-Escobar, L. (1990). The Nevados de Payachata volcanic region (18°S/69°W, N. Chile), II, evidence for widespread crustal involvement in Andean magmatism. *Contributions to Mineralogy and Petrology* **105**, 412–432.

Del Marmol, M. A. (1989). The petrology and geochemistry of Merapi Volcano, Central Java, Indonesia. Ph.D. thesis, Johns Hopkins University, Baltimore, MD.

DePaolo, D. J. (1981). Trace element and isotopic effects of combined wallrock assimilation and fractional crystallization. *Earth and Planetary Science Letters* **53**, 189–202.

Dosso, L., Vidal, P., Cantagrel, J. M., Lameyre, J., Marot, A. & Zimine, S. (1979). 'Kerguelen: continental fragment or oceanic island?'; petrology and isotopic geochemistry evidence. *Earth and Planetary Science Letters* **43**, 46–60.

Dosso, L., Bougault, H., Beuzart, P. & Calvez, J. Y. (1988). The geochemical structure of the South-East Indian Ridge. *Earth and Planetary Science Letters* **88**, 47–59.

Dupré, B. & Allègre, C. J. (1983). Pb–Sr isotope variation in Indian Ocean basalts and mixing phenomena. *Nature* **303**, 142–146.

Edwards, C. M. H., Menzies, M. A. & Thirlwall, M. F. (1991). Evidence from Muriah, Indonesia, for the interplay of supra-subduction zone and intraplate processes in the genesis of potassic alkaline magmas. *Journal of Petrology* **32**, 555–592.

Edwards, C. M. H., Morris, J. D. & Thirlwall, M. F. (1993). Separating mantle from slab signatures in arc lavas using B/Be and radiogenic isotope systematics. *Nature* **362**, 530–533.

Edwards, C. M. H., Menzies, M. A., Thirlwall, M. F., Morris, J. D., Leeman, W. P. & Harmon, R. S. (1994). The transition to potassic alkaline volcanism in island arcs: the Ringgit–Beser Complex, East Java, Indonesia. *Journal of Petrology* **35**, 1557–1595.

Ellam, R. M. & Harmon, R. S. (1990). Oxygen isotope constraints on the crustal contribution to the subduction-related magmatism of the Aeolian Islands, southern Italy. *Journal of Volcanology and Geothermal Research* **44**, 105–122.

Ellam, R. M. & Hawkesworth, C. J. (1988). Elemental and isotopic variations in subduction related basalts: evidence for a three component model. *Contributions to Mineralogy and Petrology* **98**, 72–80.

Elliott, T., Plank, T., Zindler, A., White, W. & Bourdon, B. (1997). Element transport from slab to volcanic front at the Mariana arc. *Journal of Geophysical Research* **102**, 14991–15019.

Feeley, T. C. & Davidson, J. P. (1994). Petrology of calc-alkaline lavas at Volcán Ollagüe and the origin of compositional diversity at central Andean stratovolcanoes. *Journal of Petrology* **35**, 1295–1340.

Ferrara, G., Laurenzi, M. A., Taylor, H. P., Jr, Tonarini, S. & Turi, B. (1985). Oxygen and strontium isotope studies of K-rich volcanic rocks from the Alban Hills, Italy. *Earth and Planetary Science Letters* **75**, 13–28.

Gamble, J., Woodhead, J., Wright, I. & Smith, I. (1996). Basalt and sediment geochemistry and magma petrogenesis in a transect from oceanic island arc to rifted continental margin arc: the Kermadec–Hikurangi margin, SW Pacific. *Journal of Petrology* **37**, 1523–1546.

Gamble, J. A., Christie, R. H. K., Wright, I. C. & Wysoczanski, R. J. (1997). Primitive K-rich magmas from Clark Volcano, southern Kermadec arc: a paradox in the K–depth relationship. *Canadian Mineralogist* **35**, 275–290.

Gasparon, M. & Varne, R. (1998). Crustal assimilation vs subducted sediment input in west Sunda arc volcanics: an evaluation. *Mineralogy and Petrology* **64**, 89–117.

Gasparon, M., Hilton, D. R. & Varne, R. (1994). Crustal contamination processes traced by helium isotopes: examples from the Sunda arc, Indonesia. *Earth and Planetary Science Letters* **126**, 15–22.

Gerbe, M.-C., Gourgaud, A., Sigmarsson, O., Harmon, R. S., Joron, J.-L. & Provost, A. (1992). Mineralogical and geochemical evolution of the 1982–1983 Galunggung eruption (Indonesia). *Bulletin of Volcanology* **54**, 284–298.

Gertisser, R. (2001). Gunung Merapi (Java, Indonesien): Eruptionsgeschichte und magmatische Evolution eines Hochrisiko-Vulkans. Ph.D. thesis, Universität Freiburg.

Gertisser, R. & Keller, J. (2003). Temporal variations in magma composition at Merapi Volcano (Central Java, Indonesia): magmatic cycles during the past 2,000 years of explosive activity. *Journal of Volcanology and Geothermal Research* (in press).

Gill, J. B. (1981). *Orogenic Andesites and Plate Tectonics*. Berlin: Springer.

Green, T. H., Sie, S. H., Ryan, C. G. & Cousens, D. R. (1989). Proton microprobe-determined partitioning of Nb, Ta, Zr, Sr and Y between garnet, clinopyroxene and basaltic magma at high pressure and temperature. *Chemical Geology* **74**, 201–216.

Hamelin, B. & Allègre, C. J. (1985). Large-scale regional units in the depleted upper mantle revealed by an isotope study of the South-West Indian Ridge. *Nature* **315**, 196–199.

Hamelin, B., Dupré, B. & Allègre, C. J. (1985). Pb–Sr–Nd isotopic data of Indian Ocean Ridges: new evidence of large-scale mapping of mantle heterogeneities. *Earth and Planetary Science Letters* **76**, 288–298.

Hamilton, W. (1979). Tectonics of the Indonesian region. *US Geological Survey, Professional Papers* **1078**, 1–345.

Harmon, R. S. & Hoefs, J. (1995). Oxygen isotope heterogeneity of the mantle deduced from global ^{18}O systematics of basalts from different geotectonic settings. *Contributions to Mineralogy and Petrology* **120**, 95–114.

Hart, S. R. (1984). The DUPAL anomaly: a large-scale isotopic anomaly in the southern hemisphere. *Nature* **309**, 753–756.

Hawkesworth, C. J., Gallagher, K., Hergt, J. M. & McDermott, F. (1993). Mantle and slab contributions in arc magmas. *Annual Review of Earth and Planetary Sciences* **21**, 175–204.

Hegner, E., Roddick, J. C., Fortier, S. M. & Hulbert, L. (1995*a*). Nd, Sr, Pb, Ar, and O isotopic systematics of Sturgeon Lake kimberlite, Saskatchewan, Canada: constraints on emplacement age, alteration, and source composition. *Contributions to Mineralogy and Petrology* **120**, 212–222.

Hegner, E., Walter, H. J. & Satir, M. (1995*b*). Pb–Sr–Nd isotopic compositions and trace element geochemistry of megacrysts and melilitites from the Tertiary Urach volcanic field: source composition of small volume melts under SW Germany. *Contributions to Mineralogy and Petrology* **122**, 322–335.

Hildreth, W. & Moorbath, S. (1988). Crustal contributions to arc magmatism in the Andes of Central Chile. *Contributions to Mineralogy and Petrology* **98**, 455–489.

Hilton, D. R. & Craig, H. (1989). A helium isotope transect along the Indonesian archipelago. *Nature* **342**, 906–908.

Hoogewerff, J. A., Van Bergen, M. J., Vroon, P. Z., Hertogen, J., Wordel, R., Sneyers, A., Nasution, A., Varekamp, J. C., Moens, H. L. E. & Mouchel, D. (1997). U-series, Sr–Nd–Pb isotope and trace-element systematics across an active island arc–continent collision zone: implications for element transfer at the slab–wedge interface. *Geochimica et Cosmochimica Acta* **61**, 1057–1072.

Hutchison, C. S. (1982). Indonesia. In: Thorpe, R. S. (ed.) *Orogenic Andesites*. Chichester: Wiley, pp. 307–325.

Ito, E., White, W. M. & Göpel, C. (1987). The O, Sr, Nd and Pb isotope geochemistry of MORB. *Chemical Geology* **62**, 157–176.

James, D. E. (1981). The combined use of oxygen and radiogenic isotopes as indicators of crustal contamination. *Annual Review of Earth and Planetary Sciences* **9**, 311–344.

Jarrard, R. D. (1986). Relations among subduction parameters. *Reviews of Geophysics* **24**, 217–284.

Jochum, K. P., Seufert, H. M., Spettel, B. & Palme, H. (1986). The solar-system abundances of Nb, Ta and Y, and the

relative abundances of refractory lithophile elements in differentiated planetary bodies. *Geochimica et Cosmochimica Acta* **50**, 1173–1183.

Katili, J. A. (1975). Volcanism and plate tectonics in the Indonesian island arcs. *Tectonophysics* **26**, 165–188.

Kay, R. W. (1980). Volcanic arc magmas: implications of a melting–mixing for element recycling in the crust–upper mantle system. *Journal of Geology* **88**, 497–522.

Keppler, H. (1996). Constraints from partitioning experiments on the composition of subduction-zone fluids. *Nature* **380**, 237–240.

Kogiso, T., Tatsumi, Y. & Nakano, S. (1997). Trace element transport during dehydration processes in the subducted oceanic crust: 1. experiments and implications for the origin of ocean island basalts. *Earth and Planetary Science Letters* **148**, 193–205.

Leake, B. E., Woolley, A. R., Arps, C. E. S., Birch, W. D., Gilbert, M. C., Grice, J. D., *et al*. (1997). Nomenclature of amphiboles: report of the subcommittee on amphiboles of the International Mineralogical Association Commission on New Minerals and Mineral Names. *Mineralogical Magazine* **61**, 295–321.

Le Maitre, R. W. (ed.) (2002). *Igneous Rocks. A Classification and Glossary of Terms. Recommendations of the International Union of Geological Sciences Subcommission on the Systematics of Igneous Rocks*. Cambridge: Cambridge University Press.

Liu, J., Bohlen, S. R. & Ernst, W. G. (1996). Stability of hydrous phases in subducting oceanic crust. *Earth and Planetary Science Letters* **143**, 161–171.

McCulloch, M. T. & Gamble, J. A. (1991). Geochemical and geodynamical constraints on subduction zone magmatism. *Earth and Planetary Science Letters* **102**, 358–374.

McDermott, F. & Hawkesworth, C. (1991). Th, Pb, and Sr isotope variations in young island arc volcanics and oceanic sediments. *Earth and Planetary Science Letters* **104**, 1–15.

McDermott, F., Defant, M. J., Hawkesworth, C. J., Maury, R. C. & Joron, J. L. (1993). Isotope and trace element evidence for three component mixing in the genesis of the North Luzon arc lavas (Philippines). *Contributions to Mineralogy and Petrology* **113**, 9–23.

Morimoto, N. (1988). Nomenclature of pyroxenes. *Mineralogical Magazine* **52**, 535–550.

Morris, J. D. & Hart, S. R. (1983). Isotopic and incompatible element constraints on the genesis of island arc volcanics from Cold Bay and Amak Island, Aleutians, and implications for mantle structure. *Geochimica et Cosmochimica Acta* **47**, 2015–2030.

Newhall, C. G., Bronto, S., Alloway, B., Banks, N. G., Bahar, I., Del Marmol, M. A., *et al*. (2000). 10,000 years of explosive eruptions of Merapi Volcano, Central Java: archaeological and modern implications. *Journal of Volcanology and Geothermal Research* **100**, 9–50.

Nicholls, I. A., Whitford, D. J., Harris, K. L. & Taylor, S. R. (1980). Variation in the geochemistry of mantle sources for tholeiitic and calc-alkaline mafic magmas, western Sunda volcanic arc, Indonesia. *Chemical Geology* **30**, 177–199.

Pearce, J. A. (1983). Role of the sub-continental lithosphere in magma genesis at destructive plate margins. In: Hawkesworth, C. J. & Norry, M. J. (eds) *Continental Basalts and Mantle Xenoliths*. Nantwich: Shiva, pp. 230–249.

Peate, D. W., Pearce, J. A., Hawkesworth, C. J., Colley, H., Edwards, C. M. H. & Hirose, K. (1997). Geochemical variations in Vanuatu arc lavas: the role of subducted material and a variable mantle wedge composition. *Journal of Petrology* **38**, 1331–1358.

Perfit, M. R., Gust, D. A., Bence, A. E., Arculus, R. J. & Taylor, S. R. (1980). Chemical characteristics of island-arc basalts: implications for mantle sources. *Chemical Geology* **30**, 227–256.

Plank, T. & Langmuir, C. H. (1998). The geochemical composition of subducting sediment and its consequences for the crust and mantle. *Chemical Geology* **145**, 325–394.

Price, R. C., Stewart, R. B., Woodhead, J. D. & Smith, I. E. M. (1999). Petrogenesis of high-K arc magmas: evidence from Egmont Volcano, North Island, New Zealand. *Journal of Petrology* **40**, 167–197.

Puspito, N. T. & Shimazaki, K. (1995). Mantle structure and seismotectonics of the Sunda and Banda arcs. *Tectonophysics* **251**, 215–228.

Rehkämper, M. & Hofmann, A. W. (1997). Recycled ocean crust and sediment in Indian Ocean MORB. *Earth and Planetary Science Letters* **147**, 93–106.

Simkin, T. L. & Siebert, L. (1994). *Volcanoes of the World*. Tuscon, AZ: Geoscience Press.

Stolz, A. J., Varne, R., Davies, G. R., Wheller, G. E. & Foden, J. D. (1990). Magma source components in an arc–continent collision zone: the Flores–Lembata sector, Sunda arc, Indonesia. *Contributions to Mineralogy and Petrology* **105**, 585–601.

Sun, S. S. & McDonough, W. F. (1989). Chemical and isotopic systematics of oceanic basalts: implications for mantle composition and processes. In: Saunders, A. D. & Norry, M. J. (eds) *Magmatism in the Ocean Basins*. *Geological Society, London, Special Publications* **42**, 313–345.

Tatsumi, Y. & Kogiso, T. (1997). Trace element transport during dehydration processes in the subducted oceanic crust: 2. Origin of chemical and physical characteristics in arc magmatism. *Earth and Planetary Science Letters* **148**, 207–221.

Tatsumi, Y., Hamilton, D. L. & Nesbitt, R. W. (1986). Chemical characteristics of fluid phase released from a subducted lithosphere and origin of arc magmas: evidence from high-pressure experiments and natural rocks. *Journal of Volcanology and Geothermal Research* **29**, 293–309.

Taylor, H. P., Jr (1968). The oxygen isotope geochemistry of igneous rocks. *Contributions to Mineralogy and Petrology* **19**, 1–71.

Taylor, H. P., Jr & Turi, B. (1976). High ^{18}O igneous rocks from the Tuscan magmatic province, Italy. *Contributions to Mineralogy and Petrology* **55**, 33–54.

Tera, F., Brown, L., Morris, J., Sacks, I. S., Klein, J. & Middleton, R. (1986). Sediment incorporation in island-arc magmas: inferences from ^{10}Be. *Geochimica et Cosmochimica Acta* **50**, 535–550.

Thirlwall, M. F., Graham, A. M., Arculus, R. J., Harmon, R. S. & Macpherson, C. G. (1996). Resolution of the effects of crustal assimilation, sediment subduction, and fluid transport in island arc magmas: Pb–Sr–Nd–O isotope geochemistry of Grenada, Lesser Antilles. *Geochimica et Cosmochimica Acta* **60**, 4785–4810.

Turner, S. & Foden, J. (2001). U, Th and Ra disequilibria, Sr, Nd and Pb isotope and trace element variations in Sunda arc lavas: predominance of a subducted sediment component. *Contributions to Mineralogy and Petrology* **142**, 43–57.

Van Bemmelen, R. W. (1949). *The Geology of Indonesia. Vol. 1A: General Geology*. The Hague: Government Printing Office.

Van Bergen, M. J., Vroon, P. Z., Varekamp, J. C. & Poorter, R. P. E. (1992). The origin of the potassic rock suite from Batu Tara Volcano (East Sunda Arc, Indonesia). *Lithos* **28**, 261–282.

Voight, B., Constantine, E. K., Siswowidjoyo, S. & Torley, R. (2000). Historical eruptions of Merapi Volcano, Central Java, Indonesia, 1768–1998. *Journal of Volcanology and Geothermal Research* **100**, 69–138.

Vroon, P. Z., Van Bergen, M. J., White, W. M. & Varekamp, J. C. (1993). Sr–Nd–Pb isotope systematics of the Banda arc,

Indonesia: combined subduction and assimilation of continental material. *Journal of Geophysical Research* **98**, 22349–22366.

Vroon, P. Z., Lowry, D., Van Bergen, M. J., Boyce, A. J. & Mattey, D. P. (2001). Oxygen isotope systematics of the Banda Arc: low $\delta^{18}O$ despite involvement of subducted continental material in magma genesis. *Geochimica et Cosmochimica Acta* **65**, 589–609.

Wheller, G. E., Varne, R., Foden, J. D. & Abbott, M. J. (1987). Geochemistry of Quaternary volcanism in the Sunda–Banda arc, Indonesia, and three-component genesis of island-arc basaltic magmas. *Journal of Volcanology and Geothermal Research* **32**, 137–160.

White, W. M. & Dupré, B. (1986). Sediment subduction and magma genesis in the Lesser Antilles: isotopic and trace element constraints. *Journal of Geophysical Research* **91**, 5927–5941.

White, W. M. & Hofmann, A. W. (1982). Sr and Nd isotope geochemistry of oceanic basalts and mantle evolution. *Nature* **296**, 821–825.

White, W. M. & Patchett, J. (1984). Hf–Nd–Sr isotopes and incompatible element abundances in island arcs: implications for magma origins and crust–mantle evolution. *Earth and Planetary Science Letters* **67**, 167–185.

Whitford, D. J. (1975*a*). Geochemistry and petrology of volcanic rocks from the Sunda arc, Indonesia. Ph.D. thesis, Australian National University, Canberra.

Whitford, D. J. (1975*b*). Strontium isotopic studies of the volcanic rocks of the Sunda arc, Indonesia and their petrogenetic implications. *Geochimica et Cosmochimica Acta* **39**, 1287–1302.

Whitford, D. J. & Jezek, P. A. (1982). Isotopic constraints on the role of subducted sialic material in Indonesian island-arc magmatism. *Geological Society of America Bulletin* **93**, 504–513.

Whitford, D. J. & Nicholls, I. A. (1976). Potassium variation in lavas across the Sunda arc in Java and Bali. In: Johnson, R. W. (ed.) *Volcanism in Australasia*. Amsterdam: Elsevier, pp. 63–75.

Whitford, D. J., Nicholls, I. A. & Taylor, S. R. (1979). Spatial variations in the geochemistry of Quaternary lavas across the Sunda arc in Java and Bali. *Contributions to Mineralogy and Petrology* **70**, 341–356.

Whitford, D. J., White, W. M. & Jezek, P. A. (1981). Neodymium isotopic composition of Quaternary island arc lavas from Indonesia. *Geochimica et Cosmochimica Acta* **45**, 989–995.

Widiyantoro, S. & Van der Hilst, R. (1996). Structure and evolution of lithospheric slab beneath the Sunda arc, Indonesia. *Science* **271**, 1566–1570.

Widiyantoro, S. & Van der Hilst, R. (1997). Mantle structure beneath Indonesia inferred from high-resolution tomographic imaging. *Geophysical Journal International* **130**, 167–182.

Wilson, M. (1989). *Igneous Petrogenesis: a Global Tectonic Approach*. London: Unwin Hyman.

Woodhead, J., Eggins, S. & Gamble, J. (1993). High field strength and transition element systematics in island arc and back-arc basin basalts: evidence for multi-phase melt extraction and a depleted mantle wedge. *Earth and Planetary Science Letters* **114**, 491–504.

Yang, H. J., Frey, F. A., Weis, D., Giret, A., Pyle, D. G. & Michon, G. (1998). Petrogenesis of the flood basalts forming the northern Kerguelen Archipelago: implications for the Kerguelen plume. *Journal of Petrology* **39**, 711–748.

Yiou, F. & Raisbeck, G. M. (1972). Half-life of ^{10}Be. *Physical Review Letters* **29**, 372–375.

You, C.-F., Castillo, P. R., Gieskes, J. M., Chan, L. H. & Spivack, A. J. (1996). Trace element behavior in hydrothermal experiments: implications for fluid processes at shallow depths in subduction zones. *Earth and Planetary Science Letters* **140**, 41–52.